

UNIVERSIDADE DE LISBOA
FACULDADE DE CIÊNCIAS
DEPARTAMENTO DE FÍSICA



Deformable Registration, Dose
Remapping and Summation for Head
and Neck Adaptive Radiotherapy
Applications

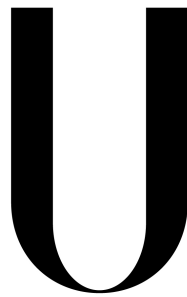
Ana Mónica Ferreira de Almeida Lourenço

Dissertação

Mestrado Integrado em Engenharia Biomédica e Biofísica
Perfil em Sinais e Imagens Médicas

2013

UNIVERSIDADE DE LISBOA
FACULDADE DE CIÊNCIAS
DEPARTAMENTO DE FÍSICA



LISBOA

UNIVERSIDADE
DE LISBOA

Deformable Registration, Dose
Remapping and Summation for Head
and Neck Adaptive Radiotherapy
Applications

Ana Mónica Ferreira de Almeida Lourenço

Dissertação

Mestrado Integrado em Engenharia Biomédica e Biofísica

Perfil em Sinais e Imagens Médicas

Orientador externo: Professor Doutor Gary Royle

Orientador interno: Professor Doutor Eduardo Ducla Soares

2013

RESUMO

Um tratamento de radioterapia tem como objectivo aplicar a dose máxima ao volume tumoral, provocando a sua morte celular, e preservar ao máximo os órgãos de risco (tecidos adjacentes saudáveis). Existem diferentes técnicas de entrega da radiação, como por exemplo, a radioterapia conformal e a radioterapia de intensidade modulada. A radioterapia conformal permite o ajuste dos múltiplos feixes de radiação à forma do alvo tumoral. Considerando múltiplos feixes à volta de um isocentro e que cada feixe tem uma fluência uniforme, então o volume da sua intersecção será uma forma convexa sem qualquer concavidade. Contudo, os volumes tumorais podem apresentar formas côncavas. A radioterapia de intensidade modulada é uma técnica de radioterapia conformal que entrega a radiação de uma forma mais precisa, reduzindo a dose emitida aos tecidos adjacentes saudáveis, e adequando as distribuições de dose a alvos que tenham formas côncavas.

Na prática clínica de radioterapia de intensidade modulada, o tratamento é planeado tendo como base imagens médicas do paciente, adquiridas antes do começo do mesmo, sendo o tratamento delineado e simulado numa única imagem de tomografia computadorizada (TC de planeamento). Deste modo, ao longo do tratamento assume-se que a localização, a geometria e o tamanho do volume tumoral e dos órgãos de risco são constantes. Contudo, durante um típico tratamento de radioterapia, que dura cerca de 5 a 7 semanas, podem ocorrer potenciais modificações anatómicas e de posicionamento do paciente. Estas variações podem ser ainda mais significativas para pacientes oncológicos de cabeça e pescoço, uma vez que, a rápida redução do volume do tumor primário, a perda de peso e as alterações na distribuição de gordura e músculo são frequentes nestes pacientes, o que pode causar significativa discordância entre a distribuição da dose planeada e aquela que está a ser efectivamente entregue, provocando toxicidade. Nestas situações, uma nova TC de planeamento é adquirida durante o tratamento e todo o processo de planeamento é repetido. Desta maneira, o replaneamento consiste num processo que consome tempo e recurso clínicos.

A radioterapia adaptativa é uma nova forma de tratamento que permite corrigir as variações anatómicas e de posicionamento sem recurso ao replaneamento. Esta técnica utiliza imagens realizadas diariamente na sala de tratamento, como por exemplo, imagens de tomografia de feixe cónico (TCFC), para reavaliar sistematicamente a localização e a forma do volume tumoral. Estas novas imagens podem ser usadas para o cálculo de distribuições de dose diária e cumulativa que incorporem as variações anatómicas e de posicionamento no planeamento do tratamento. Deste modo, a radioterapia adaptativa depende da radioterapia guiada por imagem (IGRT), da verificação constante das distribuições de dose e da adaptação do plano inicial à anatomia corrente do paciente. Os algoritmos de registro de imagens possibilitam o uso de imagens de TCFC em radioterapia adaptativa, permitindo a adaptação do plano inicial de tratamento à anatomia actual do paciente. A TC de planeamento (pTC) pode ser deformada de acordo com a TCFC, produzindo uma nova imagem (pTC deformada), que tem a qualidade de imagem da pTC mas que contém a informação estrutural da TCFC. Deste modo, aplicando as configurações dos feixes do plano inicial à anatomia da nova imagem registrada, novos cálculos de dose podem ser efectuados na imagem de pTC deformada.

O presente estudo teve como objectivo o desenvolvimento de um método para calcular a distribuição da dose cumulativa recebida por pacientes oncológicos da cabeça e pescoço ao longo dos seus tratamentos, através de avançadas técnicas de registro de imagens (usando transformadas B-Spline) que incorporam as variações anatómicas e de posicionamento que possam ocorrer. Neste estudo, foram incluídos 5 pacientes com cancro da cabeça e pescoço. Os pacientes foram tratados com radioterapia de intensidade modulada e, durante o tratamento, verificaram-se significativas variações anatómicas em todos os pacientes, o que resultou em 4 deles terem sido sujeitos a replaneamento. O processo de soma de dose utilizado consistiu no subsequente processo descrito. A imagem de pTC é registrada a uma série de imagens de TCFC adquiridas ao longo do tratamento. O *output* deste processo é uma série de transformações T que deformam a imagem de pTC de acordo com as alterações anatómicas que ocorreram no paciente. Novos cálculos de dose são realizados em cada imagem de pTC deformada, usando o plano de tratamento inicial, e as distribuições de dose são mapeadas de volta para o espaço da dose da pTC usando o inverso da transformação T^{-1} . A aplicação da transformada inversa permite mapear as novas distribuições de dose, que incorporam as modificações anatómicas e de posicionamento que possam ter ocorrido, para o mesmo referencial (espaço da dose da

pTC) possibilitando, deste modo, a sua soma. Devido há complexidade matemática que envolve a computação da inversa de uma transformada B-Spline T^{-1} , não existe solução analítica para o seu cálculo.

Este estudo teve como principal objectivo estudar e avaliar o desempenho de três diferentes métodos que estimam T^{-1} : (i) o método não-simétrico, (ii) o método simétrico (iii) e métodos de estimação iterativos. O desempenho de cada método é avaliado com base na (i) inspecção visual dos resultados do processo de registro de imagens e na (ii) computação de medidas de similaridade, que garantem a qualidade de correspondência entre as imagens, no (iii) cálculo do Jacobiano e no (iv) erro de consistência inversa que asseguram que as transformações (T e T^{-1}) são fisicamente plausíveis. Diferentes distribuições de dose, obtidas através dos diferentes métodos de computação da inversa, foram comparadas através da análise de diferenças de dose e gamma análise, e histogramas dose-volume foram gerados para estudar os efeitos dosimétricos em estruturas de interesse.

O método de estimação iterativa foi o que apresentou os resultados mais robustos em termos de consistência entre a transformada T e a transformada T^{-1} , com um erro médio de 0.009 mm. O método não simétrico apresentou um erro médio de 1.793 mm e o método simétrico um erro médio de 0.500 mm. Relativamente aos efeitos dosimétricos, os diferentes métodos de computação de T^{-1} mostraram performances semelhantes entre si. Para diferentes distribuições de dose, as curvas dos histogramas dose-volume sobrepuseram-se consideravelmente e a diferença absoluta de dose máxima em órgãos de risco foi inferior a 1.1 Gy. Os valores aqui apresentados representam valores medianos sobre todos os pacientes considerados.

Os resultados mostraram que os métodos de computação da inversa de uma transformada B-Spline têm potencial para serem utilizados no cálculo da dose cumulativa e no cálculo da dose recebida pelo paciente em cada semana do tratamento.

A dissertação encontra-se dividida em 5 grandes capítulos. O primeiro consiste numa introdução ao tema da dissertação e no segundo são descritos os principais conceitos inerentes ao trabalho desenvolvido, como por exemplo, conceitos de radioterapia, planeamento e registro de imagens. São também descritos os diferentes algoritmos considerados e os métodos utilizados no seu processo de validação. O terceiro capítulo descreve os materiais e as metodologias utilizadas e o quarto os resultados obtidos. Discussão e conclusões encontram-se no quinto capítulo.

Palavras-chave: Radioterapia Adaptativa, Registro de imagens, Soma da dose, transformada B-Spline, inversa da transformada B-Spline

ABSTRACT

Purpose

The aim of this study was to assess and evaluate different methods of computing the inverse of a B-Spline transformation in order to calculate the cumulative doses received by head and neck (HN) cancer patients while accounting for variable anatomy.

Materials and Methods

Five patients with HN cancer were treated with IMRT and 4 of them were replanned midtreatment. Planning CT scan and CBCT image taken before replan were available. Planning CT images were registered to the CBCT scans and new dose calculations were performed in the deformed pCT images using the treatment IMRT plan. Dose distributions were mapped back to the pCT dose space using different methods of computing the inverse of a B-Spline transformation: (i) non-symmetric, (ii) symmetric and (iii) estimate the inverse methods. Their performance was evaluated based on visual inspection of registration results and computation of similarity measures, deformation field analysis and calculation of the inverse consistent error between the composition of forward and inverse transformations. Furthermore, dose comparisons were performed using dose difference (DD) and gamma analysis and dose volume histograms (DVH) were generated to study the dosimetric effects.

Results

Estimating the inverse methods gave the most robust results in terms of inverse-consistency between the composition of forward and inverse transformations with a median mean IC error of 0.009 mm. Regarding the dosimetric effects, results were found to be consistent between different inverse transforms. DVHs overlapped considerably and median values for maximum absolute dose differences in organs at risk were found to be less than 1.1 Gy.

Conclusion

Recalculated dose distributions in a deformed pCT can be mapped back to the pCT dose space using different methods of computing the inverse of a B-Spline transformation, allowing the calculation of cumulative doses while accounting for anatomic variations.

Key-words: Adaptive Radiotherapy, Deformable Registration, Dose summation, B-Spline Transform, Inverse of a B-Spline transform

ACKNOWLEDGMENTS

I would like to express my gratitude to everyone who made my stay in the University College London (UCL) so special and rewarding, there are no words to describe how happy and proud I am to have met them and to have had the opportunity to contact and work with them.

Firstly, I must thank to my supervisor **Gary Royle**, from the University College London (UCL) who gave me the opportunity to go abroad and this project. I also want to thank him for his clear guidance, generosity and encouragement and for always being available, I appreciate his vast knowledge and skill in many areas. A special thank to **Jamie McClelland** and **Catarina Veiga** who were so patient and glad to teach me everything I wanted to know even though they are very busy with their work, they always found a time for me. Their dedication, expertise, understanding and patience added considerably to my project. I have the most respect for them and they are an inspiration to me as scientists and human beings.

I would also like to thank very much to **Marcel Van Herk** who provided me the estimate 1 inverse transform code which was crucial to the success of this project.

Also a big thank you to all the staff of the **Radiotherapy Physics group** from University College London Hospital who so well received me and provided me the data I needed for this project.

I am deeply thankful and I want to express a very special thanks to **Professor Eduardo Ducla Soares** for his guidance and encouragement during the time I have been his student in the Faculty of Sciences of the University of Lisbon. His unceasing support and motivation were crucial for my achievements in the last 5 years.

A big thank you to all my friends in the **Radiation Physics group**

from University College London who received me so well and who made me enjoy much more my stay in London. I would specifically like to thank **Andria, Dan, Tasos, Catarina, Ireneos** and **Tania** for their friendship and for the great moments and happy times we spent together. I also would like to thank **Paul, Marco, Joanna** and **Charlotte** for being part of our running club, especially **George** and **Tom** which adventure spirit inspired me.

In addition, a very special thanks to my Stockwell's family, **Rui, Sara** and **Andreia** for being the family I needed when I was miles away from home. And also to my London friends, **Joanna** and **António**, for their friendship, love and wise advices.

There are no words to describe how grateful I am to my wonderful parents **Maria** and **Júlio**, my sisters **Cátia** and **Júlia**, my aunt **Gotty** and my cousin **Rafa**, and my friends **Inês, Andrade, Maria, Mariana** and **Rita** who always support me and were always by my side.

CONTENTS

Resumo	i
Abstract	v
Acknowledgements	vii
List of Tables	xii
List of Figures	xiii
List of Abbreviation	xv
1 Introduction	1
2 Background	3
2.1 Radiotherapy	3
2.1.1 Intensity modulated radiation therapy	3
2.1.1.1 Volumetric modulated arc therapy	4
2.1.2 Adaptive Radiotherapy	4
2.1.3 Current practice of a Radiotherapy treatment at Uni- versity College London Hospital	5
2.1.3.1 Volume delineation	6
2.1.3.2 Computed tomography	8
2.1.3.3 Cone beam computed tomography	8
2.2 Medical image registration	9
2.2.1 Transformation models	9
2.2.1.1 Rigid transformations	9
2.2.1.2 Non-rigid transformations	10
2.2.1.3 B-Spline transformation	11
2.2.1.3.1 B-Spline Curves	11
2.2.1.4 B-Spline interpolation	12

CONTENTS

2.2.2	Inverse transformation models	14
2.2.2.1	Asymmetric transformation	15
2.2.2.2	Symmetric inverse consistent transformation	15
2.2.2.3	Estimating the inverse of a B-Spline transformation	16
2.2.3	Validation process: quality criteria	17
2.2.3.1	Image matching quality	17
2.2.3.1.1	Visual assessment	17
2.2.3.1.2	Similarity measures	18
2.2.3.2	Deformation field analysis	20
2.2.3.2.1	Jacobian	20
2.2.3.2.2	Inverse consistent error	20
2.2.4	Dose comparison	21
2.2.4.1	Relative dose difference	22
2.2.4.2	Distance-to-agreement	22
2.2.4.3	Gamma evaluation	22
2.2.4.4	Dose-volume histograms	24
2.3	Previous work	25
3	Materials and methods	27
3.1	Data sets	27
3.1.1	DICOM	27
3.2	Data Processing	28
3.2.1	Image Registration - Performed in NifTK	28
3.2.1.1	Forward asymmetric registration	29
3.2.1.2	Inverse of the transformation	30
3.2.1.2.1	Backward asymmetric registration	30
3.2.1.2.2	Symmetric registration	31
3.2.1.2.3	Estimate the inverse methods - Performed in Matlab/NifTK	31
3.2.2	Dose Calculation - Performed in Eclipse	32
3.2.3	Dose Summation - Performed in Matlab	32
3.2.4	Deformed dose - Performed in NifTK	34
3.3	Evaluation tools	35
3.3.1	Visual assessment and similarity measures	35
3.3.1.1	Forward transform	36
3.3.1.2	Inverse transform	36
3.3.1.3	Inverse consistence criterion	36
3.3.1.4	Symmetric registration	38
3.3.2	Deformation field analysis	39
3.3.3	Dosimetric measures	39

CONTENTS

4	Results	40
4.1	Symmetric registration performance	40
4.2	Evaluation of different inverse transform methods	43
4.2.1	Similarity comparison	43
4.2.2	Dosimetric comparison	49
4.3	Cumulative dose calculation	53
4.4	Comparison of deformed pCT dose and recalculated dose . . .	56
5	Discussion and conclusion	59
	Bibliography	61
	Appendix	72
A	Matlab code	72
A.1	Dose summation process	72
B	Guidelines for dose summation tool use	77

LIST OF TABLES

4.1	Symmetric registration performance. IC error results for Patient X.	41
4.2	Symmetric registration performance. IC error results for Patient X, Y and Z.	43
4.3	Registration performance in the forward direction: NMI results.	44
4.4	Registration performance in the backward direction: NMI results.	45
4.5	Inverse consistency between transformations: normalized cross correlation results shown in a table.	48
4.6	Inverse consistent error.	49
4.7	Dose comparison between different inverse transforms: dose difference and gamma tests.	50
4.8	Dose comparison between different inverse transforms: maximum absolute dose differences in organs at risk	50
4.9	Dose summation comparison between different inverse transforms: dose difference and gamma tests	53
4.10	Dose summation comparison between different inverse transforms: maximum absolute dose differences in organs at risk . .	53
4.11	Dose comparison between recalculated dose in the deformed pCT and deformed pCT dose: dose difference and gamma tests	57
4.12	Dose comparison between recalculated dose in the deformed pCT and deformed pCT dose: maximum absolute dose differences in organs at risk	57

LIST OF FIGURES

2.1	IMRT's traversing plastic blocks	4
2.2	Diagram to illustrate the main structures of interest in radio-therapy.	7
2.3	Example showing the difference between rigid and non-rigid registration.	10
2.4	Example of a displacement vector field.	11
2.5	B-Spline Basis Function.	12
2.6	B-Spline curves with different values of scaling factors.	12
2.7	2D example of a B-Spline control-point grid superimposed upon an aligned voxel grid.	13
2.8	Example of a deformed grid in registration.	13
2.9	Schematization of a deformable registration performed in the forward direction.	15
2.10	Schematization of a deformable registration performed in the backward direction.	16
2.11	Schematization of a symmetric deformable image registration.	16
2.12	Example of a bad and a good registration.	17
2.13	Representation of the entropies involved in mutual information theory.	18
2.14	Effect of the Jacobian in registration.	21
2.15	Schematization of the inverse consistent error.	21
2.16	Geometric representation of the gamma combined acceptance criterion of dose difference and distance-to-agreement test for 2D dose distributions.	23
2.17	Differential and cumulative DVHs.	24
3.1	External Beam Planning from Eclipse System.	33
3.2	Dose summation process.	34
3.3	Deformed dose process.	35
3.4	Forward direction transformations.	36
3.5	Backward direction transformations.	37

LIST OF FIGURES

3.6	Inverse consistency test.	37
3.7	Evaluation of the symmetric algorithm proposed.	38
4.1	Symmetric registration performance. Transverse plane images of Patient X.	42
4.2	Registration performance in the forward direction: coronal plane images example.	44
4.3	Registration performance in the backward direction: coronal plane images example.	46
4.4	Inverse consistency between transformations: coronal plane intensity difference images.	46
4.5	Inverse consistency between transformations: normalized cross correlation results shown in a graph.	47
4.6	Inverse consistency between transformations: sum of squared intensity differences results.	48
4.7	DVHs curves for different methods of computing the inverse.	52
4.8	Inverse consistency between transformations: coronal plane dose difference images.	54
4.9	DVHs curves for different methods of computing the inverse in dose summation.	55
4.10	Comparison between DVHs curves for recalculated dose in the deformed pCT and deformed pCT dose.	58

LIST OF ABBREVIATIONS

3D Three-dimensional.

ART Adaptive radiotherapy.

BE Bending energy.

CBCT Cone beam computed tomography.

CFRT Conformal radiotherapy.

CT Computed Tomography.

CTV Clinical target volume.

DD Dose difference.

DICOM Digital Imaging and Communication in Medicine.

DIR Deformable image registration.

DOF Degrees of freedom.

DTA Distance-to-agreement.

DVH Dose-volume histogram.

FoV Field of view.

GTV Gross target volume.

Gy Gray.

HN Head and neck.

List of Abbreviations

HU Hounsfield unit.

IC Inverse consistent.

IMRT Intensity modulated radiation therapy.

kV Kilovoltage.

MI Mutual information.

MR Magnetic resonance.

NCC Normalized cross correlation.

NIfTI Neuroimaging informatics technology initiative.

NMI Normalized mutual information.

OAR Organ at risk.

pCT Planning computed tomography.

pD Prescribed dose.

PET Positron emission tomography.

PRV Planning risk volume.

PTV Planning target volume.

QA Quality assurance.

RT Radiotherapy.

SIC Symmetric inverse consistent.

SSD Sum of squared intensity differences.

UCLH University College London Hospital.

VMAT Volumetric modulated arc therapy.

VOI Volume of interest.

CHAPTER 1

INTRODUCTION

Radiotherapy is a cancer treatment widely used in head and neck (HN) cancer patients. They potentially benefit from intensity modulated radiation therapy (IMRT) which conforms the dose to target volumes with complex shapes whereas avoiding critical structures (organs at risk) in close proximity of tumour targets. However, in current practice of IMRT, treatments are planned in only one planning computed tomography (pCT) taken before the course of treatment therefore potential modifications of the patient's anatomy and positioning may occur during a typical 5 to 7 weeks of treatment, leading to a significant disagreement between the dose distribution planned and the dose distribution that is actually delivered. Therefore a new CT scan can be acquired midtreatment and be used to replan the patient. Nevertheless, replan is a very time consuming process with a high-workload clinical settings [1]. Adaptive radiotherapy (ART) is a possible solution to overcome these limitations. It uses daily imaging, such as cone beam computed tomography (CBCT), performed in the treatment room to systematically reassess tumour current location and its shape and it permits the calculation of daily and cumulative dose distributions over time which incorporate anatomical and positioning variations into the treatment planning [2],[3],[4].

Deformable image registration (DIR) algorithms make possible to use CBCT images in ART by adapting the treatment plan to the current patient's anatomy. Planning CT scan can be deformed to match the CBCT image, producing a new image set (deformed pCT) which has the image quality of the pCT and the structural information of the CBCT image. Therefore new dose calculations can be conducted on the deformed pCT by applying the beam configurations of the initial plan to the anatomy of the

new image registered [5].

In this study, we propose a method to compute the cumulative dose distribution received by radiotherapy HN patients while accounting for anatomical variations using advanced deformable registration techniques. Planning CT image is registered to a series of CBCT images obtained over the course of the treatment, producing a transformation (T) which deforms the pCT according to the anatomic changes that occurred in the patient. New dose calculations are performed in each deformed pCT and dose distributions are mapped back to the pCT dose space using the inverse of the transformation (T^{-1}), in order to have all the dose distributions in the same referential (pCT dose space) and then to sum them. The aim of this study is to assess and evaluate different methods of computing T^{-1} . Their performance was evaluated based on visual inspection of registration results and computation of similarity measures to ensure image matching quality, deformation field analysis and calculation of the inverse consistent error to ensure that transformations are physically plausible. Furthermore, dose comparisons are evaluated using dose difference (DD) and gamma analysis and dose volume histograms (DVH) are generated to study the dosimetric effects.

This dissertation is organized in the following way. Chapter 2 provides background information about clinical practice of radiotherapy image, registration algorithms used and their evaluation process and it also summarises the work already done in the previous project stage. Chapter 3 describes the data, software and methodologies used and chapter 4 presents the results obtained. Chapter 5 summarises and discusses its findings and contributions, future work arising from this study and concluding remarks.

CHAPTER 2

BACKGROUND

2.1 RADIOTHERAPY

The aim of a radiotherapy (RT) treatment is to deliver the maximum dose to a tumour target while minimizing dose to normal tissues. Different delivery methods have been used [6]. Conformal radiotherapy (CFRT) consists on shaping the multiple beams to conform to the shape of the tumour target. Considering the multiple beams together around an isocentre and that each beam has an uniform fluence, then the volume of their intersection will be a convex volume without any concavities [7]. This is a limitation of CFRT since tumour targets can have concave shapes. Intensity-modulated radiation therapy (IMRT) is a special form of CFRT which delivers radiation more precisely to the tumour and it reduces the dose to surrounding normal tissues allowing to conform the dose distributions to targets that have concave shapes [8].

2.1.1 INTENSITY MODULATED RADIATION THERAPY

In IMRT the radiation is delivered via fields that have non-uniform radiation fluence ¹ over its cross section. This can be achieved by traversing a plastic block through the beam (figure 2.14) which now usually done using multi-leaf collimators (MLCs). [10],[11],[7],.

IMRT plans are designed using an inverse planning process which starts with a desired dose distribution and then finds the required non-uniform

¹Radiation fluence is a quantity which describes a monoenergetic ionizing radiation beam [9].

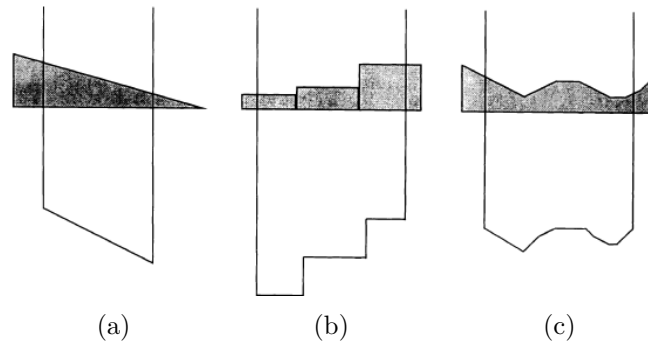


Figure 2.1: IMRT produces more complex fluence profiles by traversing objects through the beam: (a) wedges, (b) partial transmission blocks and (c) compensators [10].

fluence to create it. In other words, instead of trying a variety of configurations of possible treatments until a suitable match is found to the dose prescription, the reverse is attempted and so most IMRT planning systems optimize the intensity maps for a given number of fixed beam positions [7].

2.1.1.1 VOLUMETRIC MODULATED ARC THERAPY

It is a new delivery method which has recently become available. It consists on the delivery of IMRT beams whereas the gantry of a linac is in rotation through one or more arcs. A number of parameters can be varied like dose rate, gantry rotation speed and number of arcs. VMAT increases delivery efficiency and treatment speed [12],[13].

2.1.2 ADAPTIVE RADIOTHERAPY

IMRT treatments are based on three-dimensional (3D) imaging acquired before the start of the treatment and on each daily treatment it is assumed that location, geometry, and size of tumour and normal organs are still the same as in the planning stage [14]. However, during a typical 5-7 week radiotherapy treatment course potential modifications of the patient's anatomy and positioning can occur [15]. In head and neck (HN) patients these modifications are even more significant due to the shrinkage of primary tumour and nodal volumes, weight loss and alteration in muscle and fat

distribution, inducing a potential dosimetric impact [16].

Adaptive radiotherapy (ART) permits to correct anatomic and positioning changes as a result of the treatment [14]. It uses daily imaging performed in the treatment room to systematically reassess tumour location and shape and normal anatomy. Therefore ART is implemented based on image guidance, dose verification, and plan adaptation [17].

2.1.3 CURRENT PRACTICE OF A RADIOTHERAPY TREATMENT AT UNIVERSITY COLLEGE LONDON HOSPITAL

HN patients are one of the most sensitive cohort in radiotherapy treatments in University College London Hospital (UCLH) due to all the issues described in section 2.1.2.

IMRT and VMAT are used to treat HN cancer patients in UCLH. Radiotherapy is administrated in 30 daily fractions for a total dose of 65 gray (Gy).

Prior to treatment, a personalized patient's immobilization mask is made, in order to create a patient's reproducible position during the course of the treatment for its accuracy. Immobilization masks are made of a flat thermoplastic material that becomes deformable when warmed up with hot water. Then, the deformable thermoplastic material is placed over patient's face in the treatment position and it is attached to the treatment table to fixate the patient. The mask is deformed to patient's shape and it takes around 5 minutes to become stiff again. The patient will then wear the mask everyday for treatment.

When the mask is made the patient has a computed tomography (CT) scan using the mask in the treatment position. The alignment of the patient is done using marks drawn on the mask and a system of in-room lasers which are aligned with the CT scan and treatment gantry.

The CT scan (planning CT) is used to create the treatment plan. This process takes approximately 2 weeks and it consists on: delineation of targets and organs at risk (section 2.1.3.1), selection of beam energy, number and direction, optimization of dose distributions, assessment of dose-volume histograms (DVHs) and quality assurance (QA).

When the patient is being treated the radiographers position the patient in the treatment couch with the immobilization device attached to the table and with a support for legs and neck. Then, the radiographers shift the couch to make the system of lasers match the gantry and the initial set-up.

Outside the treatment room a daily kilovoltage (kV) imaging is acquired to improve the accuracy and efficiency of IMRT patient position verification. The radiographers check if bony anatomy matches the planning CT (pCT) and an extra couch shift can be applied.

Off-line set-up verification is assessed with a weekly cone beam computed tomography (CBCT) scan. The radiographers ensures that geometrically the planning target volume (PTV) is properly covered by the IMRT fields and CBCT images are not used for new dose calculations.

HN patients are likely to suffer appreciable anatomical changes such as weight loss due to difficulties in swallowing and tumour shrinkage. Such anatomical changes can have a negative dosimetric impact with potential overdosing to the OARs and underdosing to the tumour [1],[18],[19],[20],[21].

Replanning is done when expressive anatomical changes are seen and mask stops fitting. Replanning is only considered when no other option is viable since current replanning protocol consists on repeating all the treatment planning process increasing time and clinical resources. Replanning is also done without advanced image registration techniques to evaluate patient evolution therefore the actual dose which is being given to the patient can be considerably different from the original plan. Furthermore, it would be useful to use the daily and cumulative doses to determine when the original plan is no longer appropriate and replanning is needed (rather than trying to guess when a replan is needed based on anatomical changes).

2.1.3.1 VOLUME DELINEATION

Based on the information given by different image modalities, e.g. CT, MRI, PET, some structures of interest are contoured by a physician. The main volumes considered are:

- GTV - Gross target volume
- CTV - Clinical target volume

- PTV - Planning target volume
- OAR - Organ at risk
- PRV - Planning risk volume

The GTV consists on the gross palpable, visible, or imaged tumour tissue. CTV contains the GTV plus a margin of tissue suspected to contain microscopic tumour which therefore can not be imaged. The PTV surrounds the CTV plus a margin to account uncertainties in patient positioning or internal movement and set-up errors.

OARs are critical normal tissue structures which might be significantly damaged by the radiation such as brainstem, spinal canal and parotid glands. There are guidelines that must be followed with tolerance levels for each critical structure. PRV is a margin around OARs which accounts set-up errors and internal movement. Figure 2.2 represents a diagram which illustrates the main volumes considered in radiotherapy [22],[23],[24],[11].

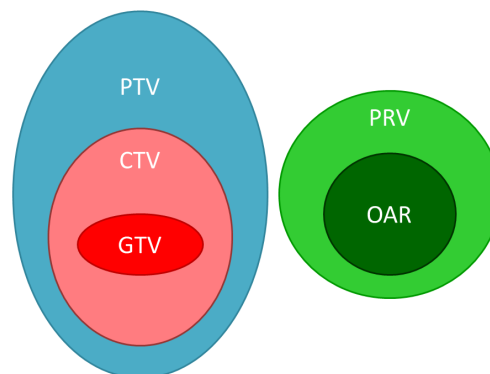


Figure 2.2: Diagram to illustrate the main structures of interest in radiotherapy [23].

Potential modifications of patient's anatomy can occur over the treatment course and the delineation of structures may not match anymore with the current patient's anatomy. ART plays a critical role to overcome this limitation by adapting the structures to the actual anatomy of the patient.

2.1.3.2 COMPUTED TOMOGRAPHY

Computed Tomography (CT) is a non-invasive type of radiography to generate cross-sectional images (slices) of the body. Images are acquired by rotating the X-ray tube 360° around the patient generating three-dimensional information about his anatomy. The radiation transmitted is measured by a ring of sensitive radiation detectors located on the gantry.

Each pixel is assigned with a CT number that is related with the linear X-ray absorption coefficient μ of the tissue at a given point:

$$\text{CT number} = 1000 \times \frac{\mu - \mu_w}{\mu_w} \quad (2.1)$$

Where μ_w is the linear attenuation coefficient of water.

CT numbers are displayed on a scale of arbitrary units named Hounsfield unit (HU) where water is assigned with 0HU. Each number represents a shade of grey with +1000 representing white (bone structures) and -1000 representing black (air) [25],[11].

2.1.3.3 CONE BEAM COMPUTED TOMOGRAPHY

Cone beam computed tomography (CBCT) is based on a cone-shaped X-ray beam mounted on the treatment gantry and a flat-panel detector. Images are acquired by rotating the source-detector system around the object. These images are used for positioning correction by comparing them with the planning CT [26],[11].

The use of CBCT images for adaptive radiotherapy is being developed for treatment planning and dose calculation. It would avoid repeated CT imaging which would reduce radiation dose to the patient and the workload to clinical staff since patient is imaged and treated in the same position. Moreover, the main advantage of CBCT acquisition is that it can be attached to the treatment machine and so acquired with the patient setup ready for treatment. However, less number of projections are acquired therefore less information is available for image reconstruction (artefacts more pronounced, image quality inferior, small field of view). Also CT values of a CBCT can not directly be used for dose calculations [26].

2.2 MEDICAL IMAGE REGISTRATION

Medical image registration is the process of matching multiple images and it is used within health care for diagnosis, planning treatment, guiding treatment and monitoring disease progression. For that, multiple images are acquired from patients at different times and often with different imaging modalities [27].

The aim of the process is to find the optimal spatial transformation T that maps one image to another:

$$T(x_B) = x_A \quad (2.2)$$

Where x_A is a point in image A and x_B is a point in image B . Two images are taken as input: A is usually called reference image and B floating image. The transformation warps the points of the floating image with the corresponding points of the reference image and so the transformation is defined on the reference image coordinate system [27].

Image registration algorithms are a key component for adaptive radiotherapy applications that automatically identify and quantify changes within the images and can be used for radiotherapy planning and treatment verification, automatic segmentation, dose tracking and summation [27],[28].

2.2.1 TRANSFORMATION MODELS

The transformation T can be characterized by different spatial transformation models according to the registration problem and it can be categorized conforming to the number of degrees of freedom (DOF). The transformation is optimized using a similarity measure through an iterative process [27]. There are a lot of different transformations and in sections 2.2.1.1 and 2.2.1.3 the most relevant for this work are explained.

2.2.1.1 RIGID TRANSFORMATIONS

It is related with the rigid behaviour of body structures like bones. It preserves distances and angles and has six degrees of freedom (DOF): three from translation and three from rotation. Rigid registration is used for motion correction in radiotherapy treatments [11],[27].

2.2.1.2 NON-RIGID TRANSFORMATIONS

In non-rigid transformations (or deformable registrations), the transformation contains localized non-rigid stretching. Deformable image registration (DIR) can be used in many applications once it can reproduce the non-rigid behaviour of the human body (examples: lungs and breast). It requires more complex algorithms than rigid transformation and it involves the determination of a large number of parameters [29],[30]. Figure 2.3 shows the difference between rigid and non-rigid registration.

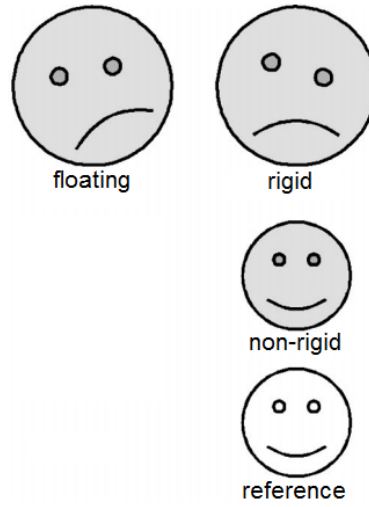


Figure 2.3: Example showing the difference between rigid and non-rigid registration. Rigid registration consists on a rigid alignment between floating and reference images. Non-rigid registration contains non-rigid stretching and it has the same internal structure of the reference but the intensity values of the floating image [30].

The goal in registration is to find the optimal transformation, $T : (x, y, z) \rightarrow (x', y', z')$, which maps any voxel in the reference image $R(x, y, z)$ to its corresponding voxel in the floating image $F(x', y', z')$ and so the key point is to find the following transformation [31]:

$$T : (x', y', z') = (x, y, z) + (u_x(x, y, z) + u_y(x, y, z) + u_z(x, y, z)) \quad (2.3)$$

In the above equation, we want to find the displacement vector field $u(\mathbf{x})$ which can be calculated using B-Spline basis function. The displacement vector field is the vector field which includes all displacement vectors of all the voxels. Looking at figure 2.4 we can easily understand equation 2.3. It represents an example of a displacement vector field where \mathbf{x} is a pixel

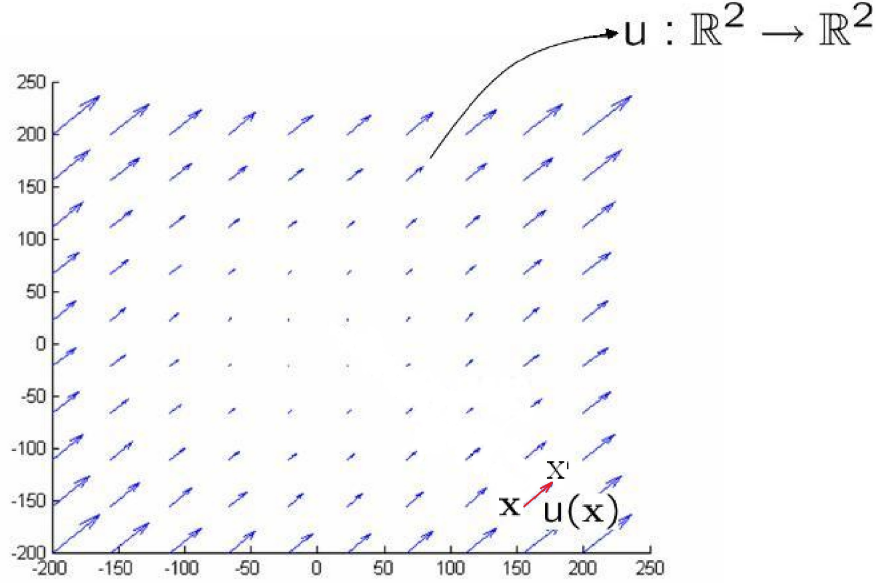


Figure 2.4: Displacement vector field [31].

in the reference image and $u(\mathbf{x})$ (in red) is the displacement function. \mathbf{x}' represents the pixel in the floating image and it comes from adding \mathbf{x} with $u(\mathbf{x})$ (equation 2.3) [31].

2.2.1.3 B-SPLINE TRANSFORMATION

There are lots of ways to parametrise a deformable transformation. B-Spline transformation is a type of non-rigid transformations and it is popular because it uses less parameters (control points) than voxels, so more efficient, but still allows for detailed deformations (how detailed depends on control point spacing) (section 2.2.1.4). It also provides some intrinsic regularisation (section 3.2.1) and it allows deformation to be easily calculated at each voxel and at any other points in the volume. Moreover, efficient implementations exist and are freely available (section 3.2.1).

2.2.1.3.1 B-SPLINE CURVES The term B-Spline is short for basis-spline and it consists on a parametric curve of a linear combination of basis B-Splines:

$$u(x) = \sum_i p_i \cdot \beta_i(x) \quad (2.4)$$

Where p_i is a spline coefficient and $\beta_i(x)$ is a piecewise spline curve [29].

B-Spline curves are used to define a continuous displacement vector field that maps the voxels in one image to those in another image [31]. In medical image registration the most common approach is to use uniform cubic B-splines curves as we can see in figure 2.5, where $\beta(x)$ is a piecewise cubic polynomial and the points $-2, -1, 0, +1, +2$ are the control points.

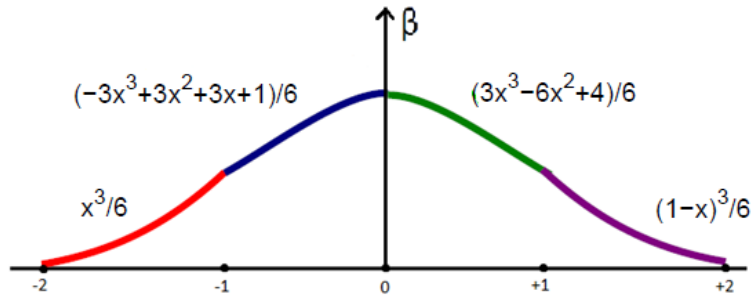


Figure 2.5: B-Spline Basis Function.

Multiplying the piecewise cubic polynomial, $\beta(x)$, for different scalar values we obtain different curves as it is shown in figure 2.6. The notation for these scaling factors is p_i and these are known for coefficient values (see equation 2.4).

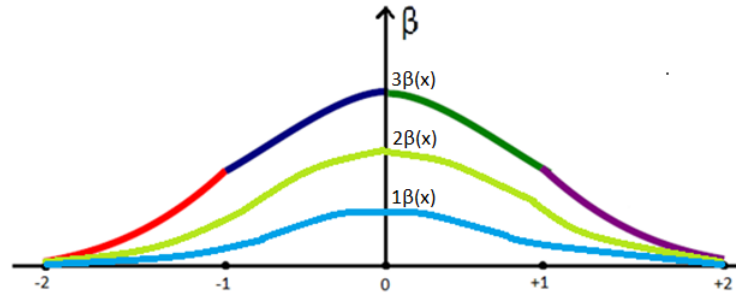


Figure 2.6: B-Spline curves with different values of scaling factors.

2.2.1.4 B-SPLINE INTERPOLATION

Figure 2.7 represents a 2D example which shows a voxel grid aligned with an uniformly spaced control grid which divides the voxel grid into 6×5 tiles (in red). The displacement vector field of the pixels within a tile is influenced

by the 16 control points in the tile's immediate vicinity [29].

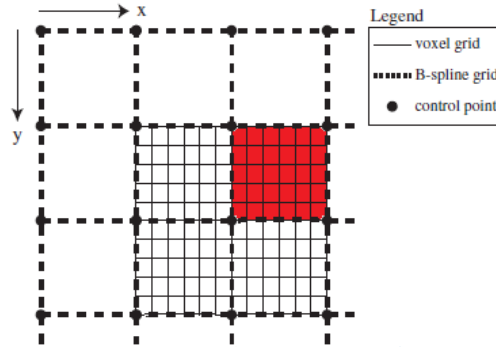


Figure 2.7: A portion of 2D image showing a B-Spline control-point grid superimposed upon an aligned voxel grid [29].

A small grid is able to align small details but the process is slow and the grid is not flexible enough for large rotations and big deformations. Figure 2.8 shows a registration performed between a square and a rectangle image. After registration, the deformed grid shows the deformation between the images.

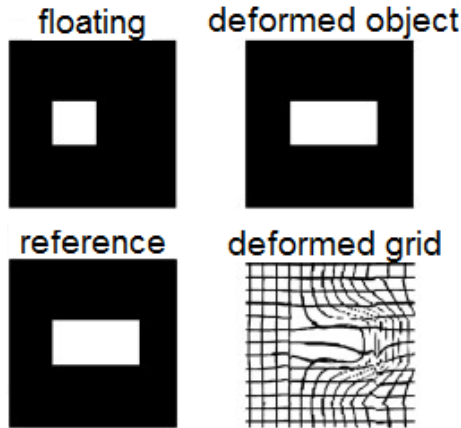


Figure 2.8: Deformed grid shows the deformation between the reference image (rectangle) and the floating image (square) [32].

Similarly, in the 3D case, the B-Spline interpolation of the x-component of the displacement vector field for a voxel located at coordinate (x, y, z)

depends on the 64 control point coefficients in the tile's immediate vicinity and it is characterized by the following equation [29]:

$$u_x(x, y, z) = \sum_{l=0}^3 \sum_{m=0}^3 \sum_{n=0}^3 \beta_l(u) \beta_m(v) \beta_n(w) p_{x,l,m,n} \quad (2.5)$$

p_x corresponds to a spline coefficient which defines the x component of the displacement vector for one of the 64 control points that influence the voxel. Positive p_i means a movement to the right (vector field points to the right) and a negative p_i means a movement to the left. If we do the registration of two identical images, we expect that all the coefficient values, p_i , would be zero [33].

The uniform cubic B-Spline basis function β_l along the x-direction is [29]:

$$\beta_l(u) = \begin{cases} \frac{(1-u)^3}{6} : l = 0 \\ \frac{(3u^3 - 6u^2 + 4)}{6} : l = 1 \\ \frac{(-3u^3 + 3u^2 + 3u + 1)}{6} : l = 2 \\ \frac{u^3}{6} : l = 3. \end{cases} \quad (2.6)$$

And similarly for β_m and β_n along the y- and z-directions, respectively [29].

Once the displacement vector field is generated, it is used to deform each voxel in the floating image. Once deformed, the floating image is compared to the reference image in terms of similarity metrics (see section 2.2.3.1.2, 3.2.1 and 3.2.1.2.2), they are what drives the registration algorithm to find the optimal result.

2.2.2 INVERSE TRANSFORMATION MODELS

In registration we want to find the transformation that maps the voxels of the floating image with the corresponding voxels of the reference image. The transformation tells us where any voxel of the floating image 'comes from' in the reference image but it does not tell us where any voxel of the reference image 'goes to' in the floating image [34]. There is no analytic solution to calculate the inverse of the transformation, T^{-1} , however it is desirable to

know it many times, e.g. for planning tracked treatment [34], [35].

Since deformable registration methods do not compute the inverse of the interpolated transform, it is necessary to estimate it. Sections 2.2.2.1, 2.2.2.2 and 2.2.2.3 describe different methods to compute the inverse of the transformation.

2.2.2.1 ASYMMETRIC TRANSFORMATION

Figure 2.9 represents a schematization of a deformable registration which maps a CT image (floating) to a CBCT image (reference). In this work, we consider that the registration performed in this direction is the forward direction.

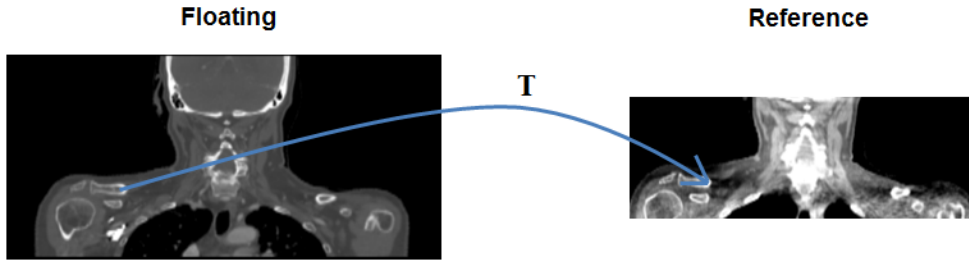


Figure 2.9: Schematization of a deformable registration performed in the forward direction which maps a CT image (floating) to a CBCT image (reference).

Unlike forward direction, backward direction maps a CBCT image (floating) to a CT image (reference) as we can see in figure 2.10. In other words, swapping our reference image with our floating image, registration is performed in the opposite direction of the forward direction.

Asymmetric backward direction transformation is independently of the transformation in the forward direction and so it can not be consider as its inverse. It is an approach which gives us an approximation of the inverse transformation.

2.2.2.2 SYMMETRIC INVERSE CONSISTENT TRANSFORMATION

In figures 2.9 and 2.10 the transformation is optimized in the forward and backward direction, respectively. Therefore the transformation is biased towards its direction. Symmetric inverse consistent (SIC) deformable image

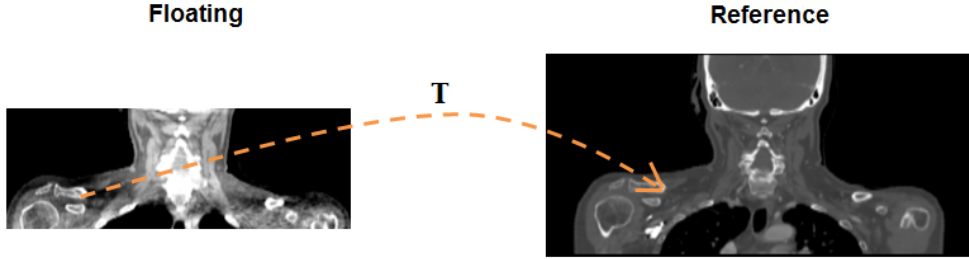


Figure 2.10: Schematization of a deformable registration performed in the backward direction which maps a CBCT image (floating) to a CT image (reference).

registration is a novel technique which optimizes both forward and backward transformation by ensuring the inverse consistency criterion (see section 2.2.3.2.2) [35],[36],[37],[38].

Figure 2.11 represents a schematization of a symmetric deformable registration.

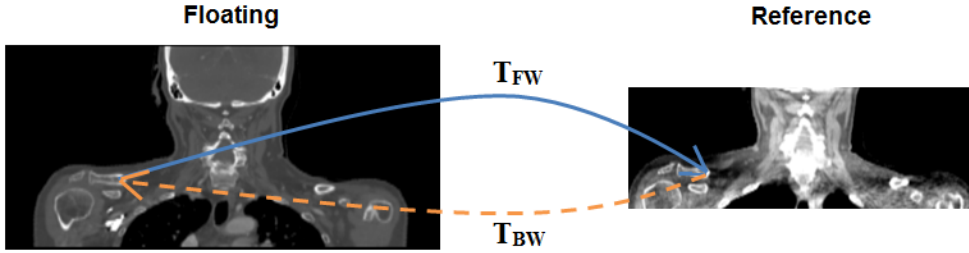


Figure 2.11: Schematization of a symmetric deformable image registration which optimizes the transformation in both directions (forward and backward).

2.2.2.3 ESTIMATING THE INVERSE OF A B-SPLINE TRANSFORMATION

It is possible to estimate the inverse of a B-Spline transformation using iterative algorithms which estimate the inverse field of a displacement vector field. The algorithms compute the inverse until it achieves a desired degree of accuracy or when they reach their iteration limit (see section 3.2.1.2.3) [34].

2.2.3 VALIDATION PROCESS: QUALITY CRITERIA

Validation of registration is particularly important in medical applications. Prior to clinical use it is mandatory to ensure that registration is correct and it is mapping the right voxels to the right places. Deformable image registration is not an exact science and its performance is patient-specific and also the lack of information to validate registration accuracy make a difficult task to decide whether registration is successful. Image matching quality and deformation field analysis are important steps to ensure it [39],[40],[41],[42].

2.2.3.1 IMAGE MATCHING QUALITY

2.2.3.1.1 VISUAL ASSESSMENT Visual inspection is a qualitative procedure of registration performance and it is an important step to registration techniques entering routine clinical use. Overlapping the reference image with the registration result is possible to infer about the image matching quality but locally implausible deformations are difficult to be detected by an expert observer [39],[41],[40]. Figures 2.12(a) and 2.12(b) represent examples of an overlap between a reference image (red) and a registration result (cyan). Registration was performed using the same reference and floating images but with different transformations and it is easy to conclude that figure 2.12(b) represents a better match than figure 2.12(a).

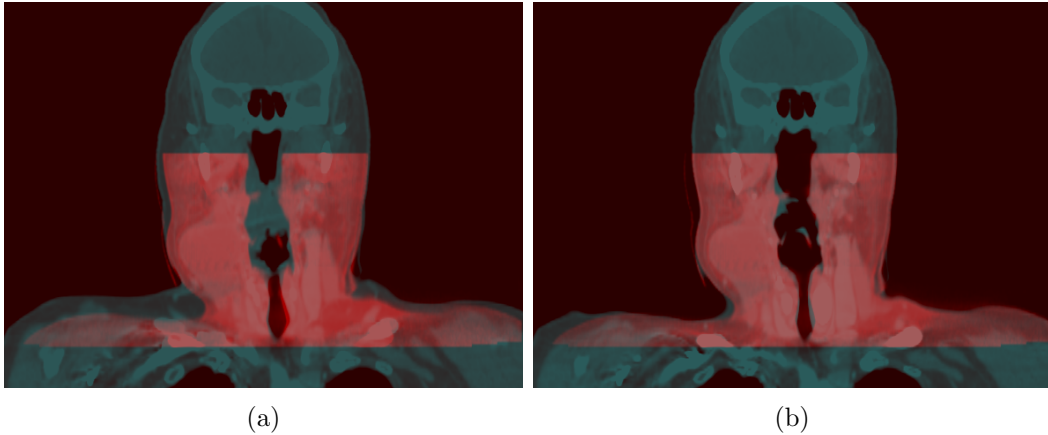


Figure 2.12: Example of a (a) bad and (b) a good registration (red: reference image; cyan: registration result). Coronal plane images.

2.2.3.1.2 SIMILARITY MEASURES Similarity measure is a quantitative measure which tells us the degree of similarity between two images. There are a large number of different similarity measures and the selection of the proper measure to use depends on the images modality and the registration goal. Normalized mutual information is a very effective measure to calculate the degree of similarity between images from different modalities such as CT and CBCT [43]. Normalized cross correlation and sum of squared intensity differences work well between images from the same modality and are easy to compute [43], [27].

NORMALIZED MUTUAL INFORMATION Mutual information (MI) measures the information shared between two images and it is maximized when they are spatially aligned. It is sensitive to changes in the size of the overlapping region therefore Studholme *et al.* [44] introduced the concept of normalized mutual information (NMI) which remains insensitive to changes in the size of background [45],[46]. It is given by [44]:

$$NMI(A, B) = \frac{H(A) + H(B)}{H(A, B)} \quad (2.7)$$

$H(A)$ and $H(B)$ are the marginal entropies of image A and B , respectively, and $H(A, B)$ the joint entropy (figure 2.13) NMI can range between 0 and 2 and values of $NMI > 1$ typically represent a good match between images.

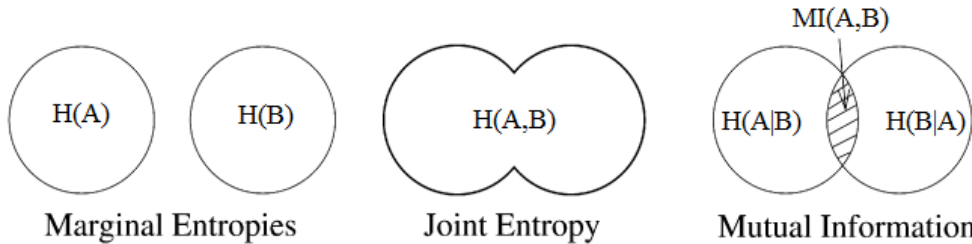


Figure 2.13: Representation of the entropies involved in mutual information theory [44].

The entropy H of a point in an image is a measure of how well the intensity at that point can be predicted [47]:

$$H(A) = - \sum_a p_A(a) \log p_A(a) \quad (2.8)$$

$$H(B) = - \sum_b p_B(b) \log p_B(b) \quad (2.9)$$

$$H(A, B) = - \sum_{a,b} p_{AB}(a, b) \log p_{AB}(a, b) \quad (2.10)$$

$p_A(a)$ is the probability that a point in image A has intensity a . The same theory is applicable for $H(B)$ and $H(A, B)$ where $p_{AB}(a, b)$ is the joint probability that a point in the overlap region has intensity a and b [39].

MI works well for intra- and inter-modality image registration. Different modalities may not have the same intensities but they always have mutual information in terms of spacial distributions.

NORMALIZED CROSS CORRELATION Normalized cross correlation (NCC) is given by the following equation:

$$NCC = \frac{\sum_{(i,j) \in \Omega} (I_A(i, j) - \bar{I}_A)(I_B(i, j) - \bar{I}_B)}{\sqrt{\sum_{(i,j) \in \Omega} (I_A(i, j) - \bar{I}_A)^2} \sqrt{\sum_{(i,j) \in \Omega} (I_B(i, j) - \bar{I}_B)^2}} \quad (2.11)$$

Where I_A and I_B are the intensity values of image A and B , respectively. \bar{I}_A and \bar{I}_B are the mean values of the images in the overlap region $(i, j) \in \Omega$.

It can takes values between -1 and +1 where +1 represents a maximum of correlation between images. NCC is very sensitive to the intensity value of a pixel therefore a small number of pixels that have large differences in intensity between images may have a big effect on the similarity measure [43].

SUM OF SQUARED INTENSITY DIFFERENCES Sum of squared intensity differences (SSD) consists on one of the simplest similarity measures and the optimal transformation is found by minimizing it:

$$SSD = \frac{1}{N} \sum_{i_A \in \Omega} |A(i_A) - B^T(i_A)|^2 \quad (2.12)$$

Where N is the number of voxels in the overlap region Ω , A is the reference image, B is the floating image, B^T is image B transformed into the coordinate space of image A and i_A is a voxel in image A .

As normalized cross correlation SSD is also very sensitive to the intensity value of a voxel.

2.2.3.2 DEFORMATION FIELD ANALYSIS

The analysis of deformation fields enables to ensure that the deformations are physically plausible (section 2.2.3.2.1) and that forward and backward transformations are inverse-consistent (section 2.2.3.2.2).

2.2.3.2.1 JACOBIAN The Jacobian matrix contains 9 values (for a 3D transformation) and describes how the transformation changes in each of the 3 directions. The determinant of the Jacobian matrix (often just called the Jacobian) gives the local volume change and both can be calculated at any point in the transformation and describe the local properties of the transform at that point.

Folding occurs when the transform causes the anatomy to fold onto itself, meaning that some points in one volume now map to two points in the other volume and some points may not map to any points. To ensure that no folding had occurred during registration the transformation must be invertible, i.e., it has an inverse. The Jacobian is an indicator of the invertibility of the transformation and it is given by the following equation:

$$J_T(\mathbf{x}) = \begin{vmatrix} \frac{\partial T_x(\mathbf{x})}{\partial x} & \frac{\partial T_x(\mathbf{x})}{\partial y} & \frac{\partial T_x(\mathbf{x})}{\partial z} \\ \frac{\partial T_y(\mathbf{x})}{\partial x} & \frac{\partial T_y(\mathbf{x})}{\partial y} & \frac{\partial T_y(\mathbf{x})}{\partial z} \\ \frac{\partial T_z(\mathbf{x})}{\partial x} & \frac{\partial T_z(\mathbf{x})}{\partial y} & \frac{\partial T_z(\mathbf{x})}{\partial z} \end{vmatrix} \quad (2.13)$$

$J_T(\mathbf{x}) = 1$ if the volume at \mathbf{x} remains the same after the transformation, $J_T(\mathbf{x}) > 1$ if there is volume expansion and $J_T(\mathbf{x}) < 1$ if there is volume shrinkage. $J_T(\mathbf{x}) \leq 0$ means that folding had occurred which is physically impossible and mathematically not invertible [44],[48].

Figure 2.14(a) shows the effect of the Jacobian in registration with a value of -35,9. It is easy to notice local foldings and twists compared with figure 2.14(b).

2.2.3.2.2 INVERSE CONSISTENT ERROR The inverse consistent (IC) error measures the degree of consistency between forward and backward transformation. Figure 2.15 represents a schematization of it where the forward transformation T_{FW} maps the point i to j and the backward transformation T_{BW} maps the point j to i' . The distance between i and i' consists on the inverse consistent error: $IC = ||i - i'||$. The optimal transformation is found minimizing d distance.[49]

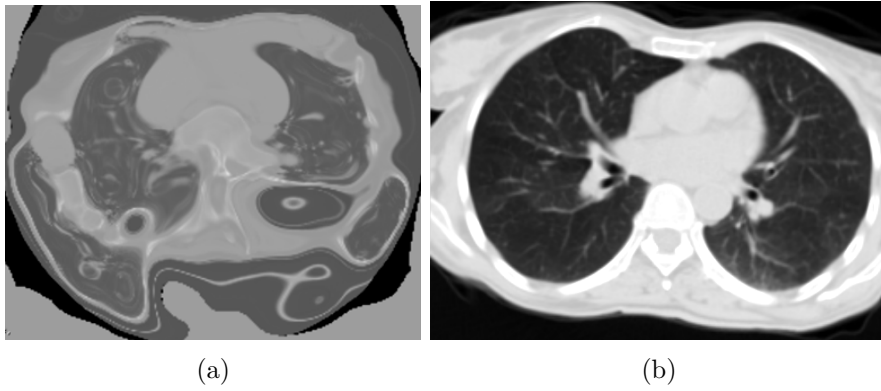


Figure 2.14: Effect of the Jacobian in registration. (a) Negative Jacobian means that folding had occurred during registration. (b) Positive Jacobian means that no folding had occurred during registration. Transversal plane images.

2.2.4 DOSE COMPARISON

Radiotherapy dose comparison plays an important rule to achieve the desired dose distribution which avoids underdosage of the target volumes (that potential increases the risk of tumour recurrence) and overdosage of normal tissues. Therefore in clinical practice it is common the comparison of two dose distributions. In sections 2.2.4.1, 2.2.4.3, 2.2.4.4 the dose comparison methods used are explained.

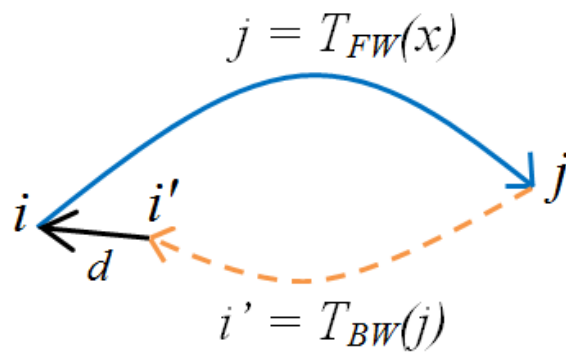


Figure 2.15: Schematization of the inverse consistent error:
 $d = \text{IC error} = ||i - i'||$

2.2.4.1 RELATIVE DOSE DIFFERENCE

Relative dose difference (DD) is the most straightforward and intuitive method which consists on the difference between two dose distributions through voxel by voxel value subtraction. Given a point r_r in the reference distribution and the corresponding point r_e in the evaluated distribution the dose difference between the two positions is $D_e(\vec{r}_e) - D_r(\vec{r}_r)$ where D represents the dose value in each point. To be able to subtract dose distributions, they must be of the same size.

In high dose gradient regions it is of less clinical significance since a large dose difference can be induced by a small alignment error [50].

A difference criterion ΔD can be set, e.g. $\Delta D = 3\%$ of the maximum dose such that points with a dose difference value greater than ΔD fail this criterion and points with a dose difference value lower than ΔD pass the criterion [51].

2.2.4.2 DISTANCE-TO-AGREEMENT

Given a point in the reference distribution r_r and the corresponding point r_e in the evaluated distribution the distance-to-agreement (DTA) corresponds to the distance between r_e and the closest point with the same dose value of r_r in the evaluated distribution:

$$DTA(\vec{r}_r) = \min|\vec{r}_e - \vec{r}_r| \quad (2.14)$$

As with dose difference (section 2.2.4.1), a DTA criterion Δd can be set. A threshold value of $\Delta d = 3mm$ is typically considered such that if the DTA at the comparison point is greater than Δd the test fails and if it is lower than Δd the test passes the criterion [51].

2.2.4.3 GAMMA EVALUATION

The gamma test combines features of both dose difference (section 2.2.4.1) and distance-to-agreement (section 2.2.4.2) tests. It was introduced by Low *et al.* [52] and its evaluation complements DD and DTA tests.

Consider two 2D dose distributions, a reference D_r and an evaluated D_e , and its points r_r and r_e , respectively. The gamma test is based on an

ellipsoid surface representing the acceptance criterion, e.g., $\Delta D = 3\%$ of the maximum dose and $\Delta d = 3mm$ of spatial tolerance, with the center located at the reference point in question \vec{r}_r [52],[51]:

$$\Gamma(\vec{r}_r, \vec{r}_e) = \sqrt{\frac{r^2(\vec{r}_r, \vec{r}_e)}{\Delta d^2} + \frac{\delta^2(\vec{r}_r, \vec{r}_e)}{\Delta D^2}} \quad (2.15)$$

Where $r(\vec{r}_r, \vec{r}_e) = |\vec{r}_e - \vec{r}_r|$ is the spatial difference between the position of the reference point \vec{r}_r and the position of the evaluated point \vec{r}_e . $\delta(\vec{r}_r, \vec{r}_e) = D_e(\vec{r}_e) - D_r(\vec{r}_r)$ represents the dose difference between the evaluate distribution D_e at position \vec{r}_e and the reference distribution D_r at position \vec{r}_r . A geometric representation of the ellipsoid can be found in figure 2.16 [52],[51].

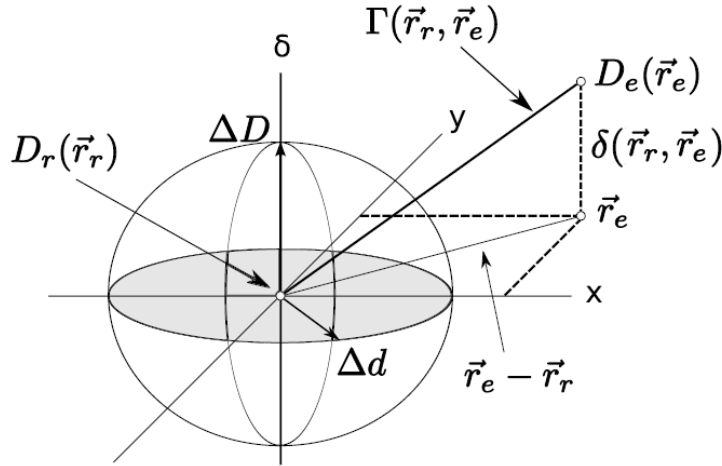


Figure 2.16: Geometric representation of the gamma combined acceptance criterion of dose difference and distance-to-agreement test for 2D dose distributions. x and y axes represent the spatial location of the point in the evaluated distribution \vec{r}_e relative to the point in the reference distribution \vec{r}_r (in the center). δ axis represents the difference in dose $D_e(\vec{r}_e) - D_r(\vec{r}_r)$. In this example point r_e fails the criterion (outside ellipsoid) [52],[51].

The gamma index is calculated by finding the minimum value of $\Gamma(\vec{r}_r, \vec{r}_e)$ varying \vec{r}_e :

$$\gamma(\vec{r}_r) = \min\{\Gamma(\vec{r}_r, \vec{r}_e)\} \forall \{\vec{r}_e\} \quad (2.16)$$

Therefore the pass-fail criteria consists on:

$$\gamma(\vec{r}_r) \leq 1, \text{ calculation passes,} \quad (2.17)$$

$$\gamma(\vec{r}_r) > 1, \text{ calculation fails.} \quad (2.18)$$

The gamma evaluation can also be applied to 3D dose distributions. For the gamma test dose distributions must have a grid resolution of $1 \times 1 \times 1$ [52].

2.2.4.4 DOSE-VOLUME HISTOGRAMS

Dose distributions within a particular volume of interest (VOI) can be summarized using dose-volume histograms (DVHs) which can be of two types: differential or cumulative DVHs.

Dose bins are represented on x axis and VOI volume on y axis. First, it is defined the range of the dose bins. In a differential DVH each bin indicates the total volume of the VOI receiving a dose within a dose range of that bin [11].

The cumulative DVH represents the volume of VOI which receives a dose greater or equal to the dose indicated on the x axis. In clinical practice cumulative DVHs are more used [11].

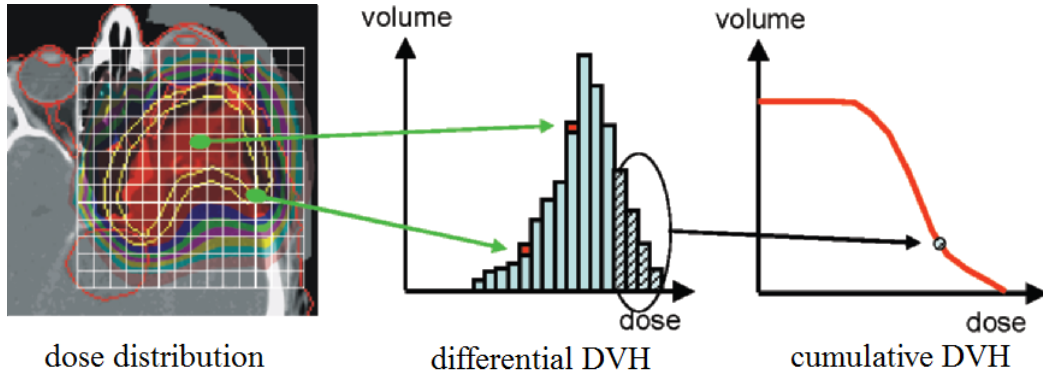


Figure 2.17: Differential and cumulative DVHs. Two voxels are identified in the dose distribution. The one in the edge of the target volume has a lower dose than the one in the center, therefore it is represented in a low dose bin compared with the other which is represented in a high dose bin in the differential DVH. In the cumulative DVH is represented the total volume of VOI which receives a dose greater or equal to the dose bin indicated [11].

2.3 PREVIOUS WORK

Different methods for estimating the cumulative dose received by radiotherapy patients while accounting for anatomic changes have been proposed. Yan *et al.* [53] using the finite element method developed a biochemical model of an elastic body to estimate organ deformations that may occurred during a radiotherapy treatment. For that purpose they used multiple daily CT images. Daily dose distributions to specific volume elements within an organ of interest were then computed while accounting for intertreatment organ deformations using registration techniques.

Rosu *et al.* [54] registered images between exhale and inhale images using thin-plate spline registration and dose distributions were computed for each data set. The transformation found between images was then direct applied to the exhale dose image and then they estimated the dose at the tracked position using trilinear interpolation from voxels in vicinity of the tracked voxel and, finally, the accumulated dose distributions were computed by summing the interpolation result with the original dose voxel value from the exhale data set.

Schaly *et al.* [55] registered multiple treatment CT studies taken throughout the treatment course to a planning CT study. Dose calculations were performed directly in the treatment studies and mapped back to the planning study using the thin-plate spline registration algorithm, allowing the fractionated dose distributions to be accumulated.

The present study makes part of a large project which has been developed between University College London (UCL) and University College London Hospital (UCLH), in order to implement adaptive radiotherapy (ART) strategies in a clinical environment for routine clinical use. ART will be a valuable tool to assist clinicians on the evaluation of off-line and online treatment procedures to account for positioning errors and anatomic changes.

The work performed by Veiga *et al.* (submitted) studied the performance of a deformable image registration (DIR) algorithm. 5 patients with HN cancer treated with IMRT who had repeat CBCT imaging and replanning over the treatment course were studied. The software was used to deform the planning CT (pCT) scan to match a CBCT image taken before replan. Two independent tests were performed to assess registration performance: (i) features manually delineated in the CBCT by a physician were compared

with features acquired automatically by warping the pCT features with the output transformation that registers the images and (ii) comparison between dose calculations for the same IMRT plan in the deformed CT and rescan CT (rCT). Features were compared using dice similarity index (DSI), overlap index (OI), centroid position error (CoM) and distance transform (DT). Dose distributions were compared based on dose difference (DD) and gamma analysis, target coverage and dose-volume histograms (DVH).

Veiga *et al.* presented a proof-of-principle for the implementation of an in-house developed deformable registration to be used in ART applications and concluded that the tool will enable the implementation of an ART procedure. They showed that a pCT can be registered to a CBCT and used to produce accurate dose calculations in the space of the CBCT volume, i.e. the dose-of-the-day. In this work we investigate warping the dose-of-the-day calculations back into a common space (the pCT space) so that they can be compared to the planned dose and each other, and the cumulative dose can be calculated and used to inform planning decisions. The same software and data used by Veiga *et al.* are used in present study and it aims to asses registration software's feasibility for dose remapping and summation.

CHAPTER 3

MATERIALS AND METHODS

3.1 DATA SETS

This study includes data from 5 HN anonymized cancer patients provided by UCLH (Patients X, Y, Z, K and S). All the patients had significant anatomic changes during the course of the treatment which resulted in 4 of them (Patients X, Y, Z, K) being re-scanned and completely replanned. All patients underwent IMRT with a planned dose of 65Gy delivered in 30 daily fractions. The data sets consists on pCT (planning CT) images acquired as part of the standard planning process of HN cancer patients at UCLH. Each pCT had associated with it (i) a set of structures (target volumes, brainstem, spinal canal and gland parotids) that had been manually identified by an expert in HN radiotherapy imaging and (ii) the treatment plan which contains information about beams energy, number and direction. For each patient who had re-plan the CBTC image taken before it was also available. Although one of the patients has not been replanned (Patient S), important weight gain and loss were observed throughout the treatment and the weekly CBCTs images acquired during the treatment course were also available.

3.1.1 DICOM

Medical imaging data sets are in DICOM (Digital Imaging and Communication in Medicine) format which is the standard format between different types of medical imaging devices. DICOM RT is specified for radiotherapy modality and it includes different types of information such as: **DICOM RT image** includes all the images acquired during the treatment and information about their position, plane and orientation; **DICOM**

RT plan has all the geometric and dosimetric data relating to treatment plan (treatment beams, dose prescription, patient setup); **DICOM RT dose** includes dose distributions calculated from the planning system and; **DICOM RT structure set** includes all the structures delineated from pCT [56].

3.2 DATA PROCESSING

The study consisted of three main parts:

- A.** DIR to map pCT image to CBCT space and map it back to planning CT space - Performed to assess different inverse transform methods for dose summation.
- B.** Dose summation - Performed to compute the weekly and cumulative dose distribution received by radiotherapy patients while accounting for anatomic variations.
- C.** Comparison of deformed pCT dose and recalculated dose in the deformed pCT - Performed to evaluate dosimetric differences between planned and recalculated dose while accounting for anatomic variations.

Three different methods of computing the inverse of the transformation T^{-1} were studied and analysed (asymmetric, symmetric and estimate the inverse methods). The 4 patients who had replan were included in this study. After that, we applied the inverse transform methods for dose summation to a clinical example (patient who had no re-plan) to illustrate the delivered dose during treatment while accounting for anatomic variations.

Of the 4 patients who had re-plan, 3 (Patients X, Y and Z) were considered for the dosimetric comparison between planned and recalculated dose.

3.2.1 IMAGE REGISTRATION - PERFORMED IN NIFTK

Registration cases were studied and solved using NifTK (<http://cmic.cs.ucl.ac.uk/home/software/>) which was developed in the Centre of Medical Image Computing (CMIC) at the Department of Medical Physics and Bioengineering of University College London (UCL). It contains of several tools such as NiftyView for image analysis and visualization and NiftyReg to perform

rigid and non-rigid registrations.

NifTK uses a common image format called NIfTI (neuroimaging informatics technology initiative) therefore NiftyView is used to convert the data sets from DICOM to NIfTI format.

Rigid registration is based on a block-matching strategy which provides a set of corresponding points between images. The process is repeated until the optimal rigid transformation is found by calculating the best correspondence between reference and floating blocks using the normalised cross correlation [57].

Deformable image registration is based on B-splines algorithm [58] to generate the displacement vector field (see section 2.2.1.3) and normalized mutual information is computed to find the best match between reference and floating image[59]:

$$NMI = \frac{H(R) + H(F(T))}{H(R, F(T))} \quad (3.1)$$

T is the deformation which maximizes the NMI between the reference R and the deformed floating $F(T)$ image. At first sight, we could think that maximizing the similarity would be the final goal of registration. However, without any restrictions, deformations can lead to unrealistic transformation results such as folding. In order to overcome these issues two penalty terms were also considered over registration: (i) the bending energy (BE) constrains the transformation to be smooth and (ii) the Jacobian (see section 2.2.3.2.1) ensures that folding not occurred [59].

Registrations were performed with an Intel Xeon CPU E25606 (2.13GHz, 12GB RAM) with a NVIDIA Tesla C2070 GPU card (14 multiprocessors, 6GB dedicated memory).

3.2.1.1 FORWARD ASYMMETRIC REGISTRATION

The pCT scan was set as floating image and the CBCT scan taken before replan was set as reference image. Replan was considered due to significant differences found between images to be registered therefore registration was performed in the worst case scenario.

A set of optimized registration parameters were previously optimized to suit the data sets being registered [60],[61]. The parameters include choice of the weight of the penalty terms such as bending energy and Jacobian. A rigid alignment was first applied followed by the deformable registration.

The registration process produced a new image set (deformed pCT) which has the image quality and HU of the pCT and the geometry information of the CBCT. CBCT image has a scan range smaller than the one for pCT and without any strategy deformed pCT will miss information about patient's anatomy. Therefore prior to registration CBCT image was extended to have the same field of view of the pCT. In the extended region the transformation results of an interpolation between the initial rigid alignment and the deformation inside of the field of view of the CBCT.

Registration procedure runs in approximately 1 minute with GPU implementation.

3.2.1.2 INVERSE OF THE TRANSFORMATION

Registration performed in the forward direction produced a transformation T which maps the pCT to the CBCT space. Three different methods of computing its inverse T^{-1} were studied. The 4 patients who had re-plan were included in this study.

3.2.1.2.1 BACKWARD ASYMMETRIC REGISTRATION Unlike forward asymmetric registration, in backward asymmetric registration the CBCT scan taken before replan was set as floating image and the pCT scan was set as reference image. The inverse rigid alignment of the forward direction was computed using NifTK and it was first applied followed by the deformable registration. Registration was performed using the same set of optimized parameters of the forward direction.

The registration process produced a new image data set (deformed CBCT) which has the image quality of the CBCT and the geometry information of the pCT.

Registration process typically takes 1 minute with GPU implementation.

3.2.1.2.2 SYMMETRIC REGISTRATION Symmetric registration was recently implemented in NifTK [38] and it optimizes forward T_{FW} and backward T_{BW} transformation (see section 2.2.2.2):

$$NMI_{SYM} = \frac{H(R) + H(F(T_{FW}))}{H(R, F(T_{FW}))} + \frac{H(R(T_{BW})) + H(F)}{H(R(T_{BW}), F)} \quad (3.2)$$

Where $H(\dots)$ are the marginal entropies and $H(\dots, \dots)$ are the the joint entropies. In order order to ensure inverse consistency between transformations a penalty term based on the inverse consistent error (see section 2.2.3.2.2) is also considered during registration.

The pCT scan was set as floating image and the CBCT scan taken before re-plan was set as reference image. A rigid alignment between images was first applied followed by the symmetric registration. The output were two geometrical transformations, forward and backward, and two new image data sets, one from registration performed in the forward direction (deformed pCT) and other from registration performed in the backward direction (deformed CBCT).

First, a set of registration parameters were optimized to suit the data sets being registered. The parameters studied included the weight of the bending energy and inverse-consistency penalty terms.

Symmetric registration is a time consuming process taking around 9 hours to run. It is not yet implemented on GPU and when it is it will be a lot faster, but still considerably slower than asymmetric registration as it considers and optimises both forward and backward transform at the same time.

3.2.1.2.3 ESTIMATE THE INVERSE METHODS - PERFORMED IN MATLAB/NIFTK Two algorithms to estimate the inverse of the forward asymmetric registration were studied and analysed:

- (i) Method 1 - Developed by Jamie McClelland [34] and performed in Matlab.
- (ii) Method 2 - Developed by Marcel Van Herk and implemented in NifTK.

Method 1 finds the inverse $i = T^{-1}(r)$ of a point r in the reference image by an iterative process. The algorithm starts with an initial estimate of the inverse i_{est} , i.e. $r_{est} = T(i_{est})$ and it computes $r - r_{est}$ until

the estimate is within the desired accuracy or the maximum number of iterations has been reached. Its estimates i_{est} based on the values of the Jacobian matrix J of the transformation T which tell us how the transformation changes in each direction [34]. Although its accuracy, it consists on a far more time consuming process taking around 2/3 days to compute the inverse of each data set, since it is implemented in MATLAB and not in C++ it is bound to be less efficient (and so time consuming).

Method 2 has the same principle as method 1 but is efficiently implemented. It computes the inverse in approximately 2 minutes with GPU implementation.

3.2.2 DOSE CALCULATION - PERFORMED IN ECLIPSE

Varian Eclipse is a treatment planning system for external beam treatment planning.

In order to import the images in NifTI format (section 3.2.1) to the treatment planning system they were first converted to DICOM format (section 3.1.1) using Matlab. It includes optimized functions that allow open, visualize and write NifTI and DICOM files.

All the information about the treatment plan (based on the planning CT and developed by a radiation oncologist) is saved on a DICOM RT plan format. This file was imported to Eclipse and it was used for dose calculations in the deformed pCT. A simulated treatment was generated by applying the beam configurations of the initial plan to the anatomy of the new image registered and calculation of dose was performed (figure 3.1). Doses were calculated using a resolution of 1 mm.

This is done to calculate the dose received by the radiotherapy patient while accounting for variable anatomy. The recalculated dose was then mapped back to the planning CT dose space using three different methods of computing the inverse to study the dosimetric difference between methods.

3.2.3 DOSE SUMMATION - PERFORMED IN MATLAB

We aimed to calculate the weekly and cumulative dose distributions received by the patient while accounting for anatomic variations. The method requires

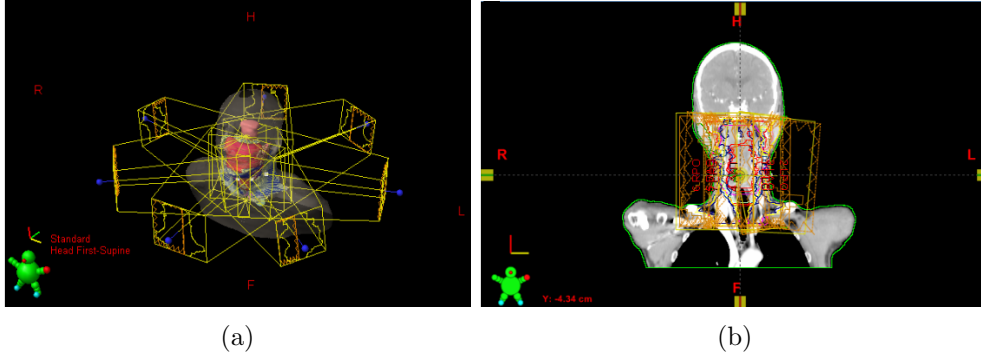


Figure 3.1: External Beam Planning from Eclipse System: (a) beam configurations of the initial plan applied to deformed pCT, (b) calculation of dose performed on deformed pCT.

a planning CT image and weekly CBCT images acquired as part of the standard planning process of HN cancer patients at UCLH. The process consists on the following steps:

- (i) Planning CT image is registered to a CBCT image. The process is repeated for each CBCT image. Each registration provides a transformation that maps the two images and a deformed pCT with the image quality and HU of the pCT and geometry information of weekly CBCT.
- (ii) Dose calculations on each deformed pCT are performed to assess the dose on a deformed anatomy in each week of the treatment.
- (iii) Map the dose distributions of each week back to the planning CT dose space.
- (iv) Dose distributions are accumulated and displayed on the planning CT dose space.

Figure 3.2 represents a schematization of the steps described above.

The contribution of each deformed pCT dose D_i is given by:

$$D_i = D_{DIR,i} \times \frac{f_i}{f_t} \quad (3.3)$$

Where $D_{DIR,i}$ is the recalculated dose in the deformed pCT, f_i the fraction at the CBCT was conducted and f_t the number total of fractions. The

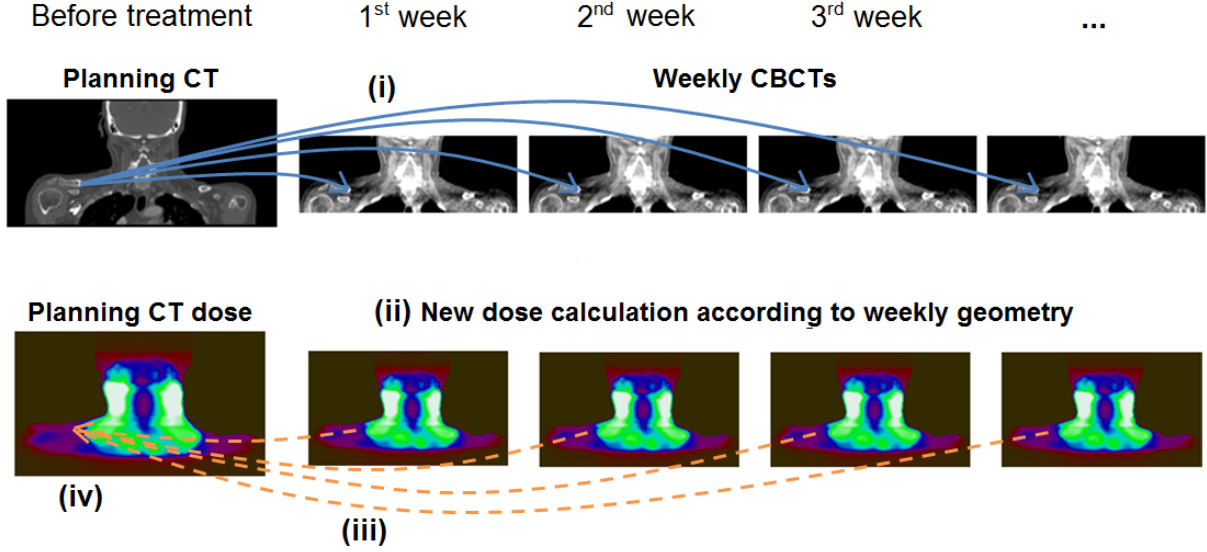


Figure 3.2: Dose summation process.

cumulative dose D_T is thus:

$$D_T = \sum_{i=1}^N D_i \quad (3.4)$$

Where N is the total number of CBCT images taken thorough treatment.

3.2.4 DEFORMED DOSE - PERFORMED IN NIFTK

The transformation that registers the planning CT to the CBCT was applied to the planning CT dose. The transformation deformed the planning CT dose according to the anatomic changes that occurred in the patient. Then the deformed planning CT dose was compared with the recalculated dose on the deformed pCT (figure 3.3).

This was done to compare the dose that we planned to give to the patient (deformed planning CT dose) with the recalculated dose and it can be used to assess the need to replan.

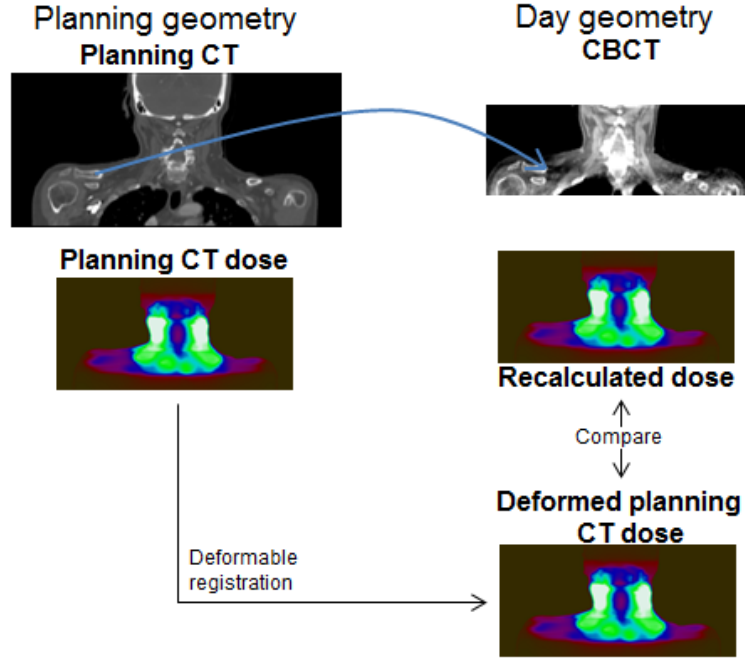


Figure 3.3: Deformed dose process.

3.3 EVALUATION TOOLS

The main focus of this thesis is the assessment and evaluation of different inverse transform methods for use in dose summation. Therefore different experiments were performed to evaluate their performance. The experiments were based on visual inspection of registration results and computation of similarity measures to ensure image matching quality, deformation field analysis to ensure that transformations were physically plausible and dose comparison (dose difference and gamma analysis, assessment of DVHs) to study the dosimetric effects. The same dosimetric measures were also applied to the substudies described in section 3.2.3 and 3.2.4.

3.3.1 VISUAL ASSESSMENT AND SIMILARITY MEASURES

Registration results were visualized and analysed using NiftyView. Evaluation consisted on the performance of the transformation T and its inverse T^{-1} . Then it was studied the inverse consistency between transformations, T and T^{-1} (section 3.3.1.3).

3.3.1.1 FORWARD TRANSFORM

Registration performed in forward direction produces a new image (deformed pCT) which has the HU of the pCT and the geometry of the CBCT (figure 3.4). Deformed pCT was compared with the CBCT image in terms of NMI since it works well for inter-modality images comparison. Two transformations were considered: $T_{FW,ASYM}$ from asymmetric registration and $T_{FW,SYM}$ from symmetric registration.

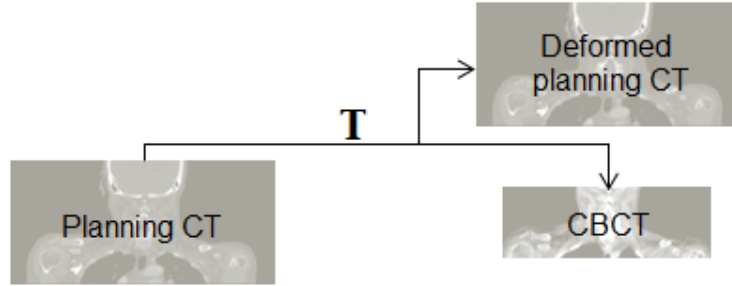


Figure 3.4: Forward direction registration can be from two transformations: (i) $T_{FW,ASYM}$ from asymmetric registration and (ii) $T_{FW,SYM}$ from symmetric registration.

3.3.1.2 INVERSE TRANSFORM

Backward direction registration produced a new image (deformed CBCT) which has the CT values of the CBCT and the geometry of the pCT image (figure 3.5). NMI was used to compute the similarity between deformed CBCT and pCT since it works well with different intensities images. Four different transformations were studied: $T_{BW,ASYM}$ from asymmetric registration, $T_{BW,SYM}$ from symmetric registration, T_1^{-1} and T_2^{-1} which estimated the inverse of $T_{FW,ASYM}$ using method 1 and method 2, respectively (section 3.2.1.2.3).

3.3.1.3 INVERSE CONSISTENCE CRITERION

In order to study the inverse consistency between forward T and inverse T^{-1} transforms, pCT was deformed by forward then backward direction generating a new image (simulated pCT) which has the HU and the geometry of the pCT. Figure 3.6 represents a scheme of the methodologies adopted. Simulated pCT was compared with pCT image using the normalized cross correlation and the sum of squared intensity differences once it is an

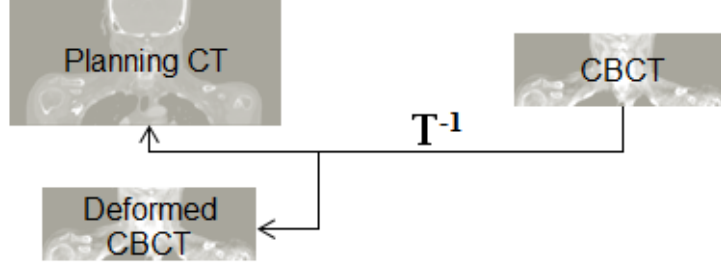


Figure 3.5: Backward direction registration can be from four transformations: (i) $T_{BW,ASYM}$ from asymmetric registration, (ii) $T_{BW,SYM}$ from symmetric registration, (iii) T_1^{-1} and (iv) T_2^{-1} which estimated the inverse of $T_{FW,ASYM}$ using method 1 and method 2, respectively.

intra-modality comparison.

Considering forward asymmetric registration $T_{FW,ASYM}$, three inverse transforms were applied to deformed pCT to map it back: $T_{BW,ASYM}$ from asymmetric registration and T_1^{-1} and T_2^{-1} which estimated the inverse of $T_{FW,ASYM}$. Therefore, for forward symmetric registration $T_{FW,SYM}$, its backward transform $T_{BW,SYM}$ was applied.

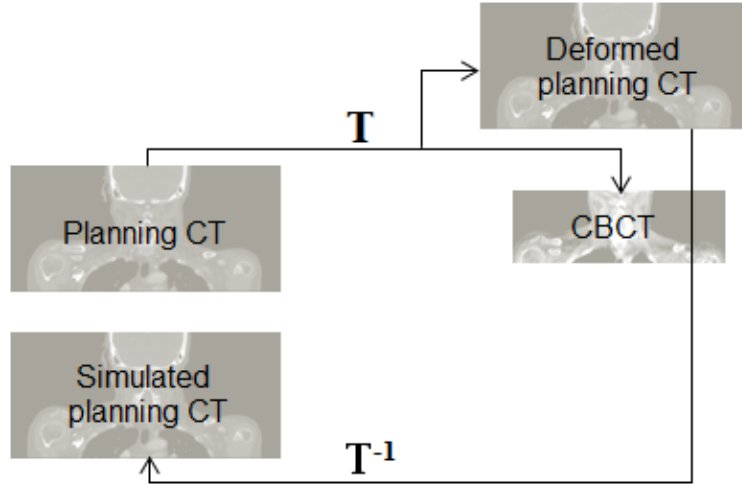


Figure 3.6: Inverse consistency test. Simulated pCT is generated using different inverse transform methods to study which inverse method gives the best approximation of the planning CT.

3.3.1.4 SYMMETRIC REGISTRATION

In theory, symmetric registration results are not biased towards the transformation direction which means that results should be the same when registration is performed from the pCT image (floating) to the CBCT image (reference) or from the CBCT image (floating) to the pCT image (reference). In order to test the symmetric algorithm, registration was performed swapping the reference with the floating image and the results were analysed using normalized cross correlation and sum of squared intensity differences. (see figure 3.7).

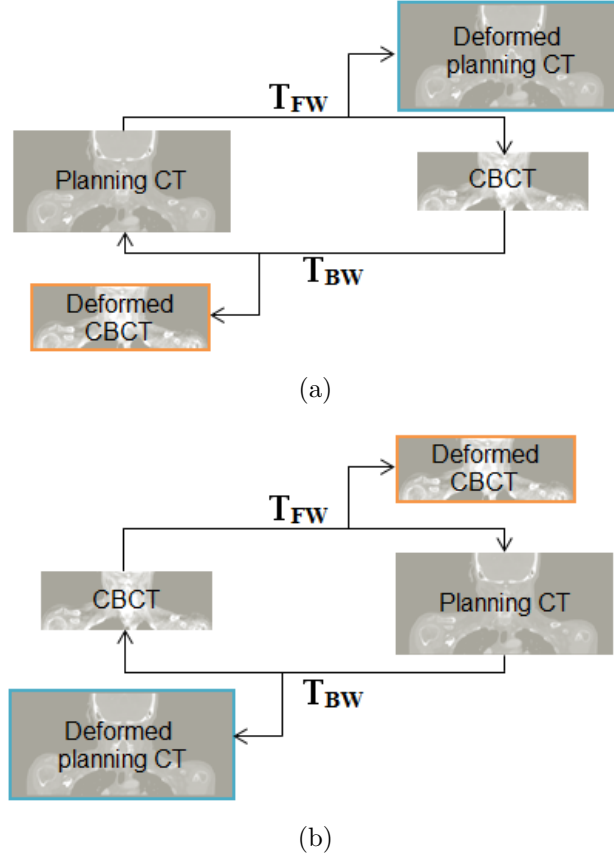


Figure 3.7: Evaluation of the symmetric algorithm proposed. Results should be the same when registration is performed (a) from the pCT image to the CBCT image or (b) from the CBCT image to the pCT image.

3.3.2 DEFORMATION FIELD ANALYSIS

The Jacobian was computed for all registrations performed in order to ensure that no folding had occurred.

The calculation of the inverse transform must ensure one-to-one mapping and generate inverse-consistent transformations. Therefore we calculated the inverse consistent error to measure the degree of consistency between forward and inverse transformations.

3.3.3 DOSIMETRIC MEASURES

Dose comparison between two 3D dose distributions was evaluated using relative dose difference and gamma analysis. DVHs were generated and analysed for each dose distribution computed.

CHAPTER 4

RESULTS

The present chapter is focused on the results from the data analysis. The chapter is divided into four main parts:

- A.** Similarity comparison to optimize symmetric registration.
- B.** Similarity and dosimetric comparison to assess different inverse transform methods.
- C.** Dosimetric evaluation to validate the dose summation process proposed.
- D.** Dosimetric comparison of deformed pCT dose and recalculated dose in the deformed pCT.

4.1 SYMMETRIC REGISTRATION PERFORMANCE

In order to test the symmetric algorithm, registration was performed from the pCT image (floating) to the CBCT image (reference) and from the CBCT image (floating) to the pCT image (reference). Symmetric registration algorithm showed to be not biased towards the transformation direction. A normalized cross correlation of 1 and a sum of squared intensity differences of 0 were found between registration results which means that the algorithm is independently of the direction of registration.

Since symmetric registration was recently implemented in NifTK, it was first required to optimize the symmetric registration parameters in order to achieve the best possible results. This was done by changing the different registration parameters and studying their effects in the registration. The parameters should be universal and give good results for all the datasets

CHAPTER 4. RESULTS

available. Of the 4 patients who had replan, 3 (Patient X, Y and Z) were included in this study. Planning CT scan and CBCT image taken before replan were available.

We started the evaluation by considering a set of previously optimized asymmetric registration parameters [60],[61] and the study was focused on the new penalty term implemented which is based on the inverse consistent (IC) error. Since symmetric registration is a time consuming process each registration was performed with a maximum number of 300 iterations (default value) instead of 1000 iterations as in [60],[61]. Computation time is reduced by reducing the maximum number of iterations since the algorithm stops before it reaches a convergence value. Jacobian penalty term constrains the transformation avoiding the occurrence of folding therefore it was set to zero in order to test if symmetric registration algorithm generates a one-to-one mapping (no folding).

The IC weight was varied from 0 to 0.5. In each registration performed the NMI between reference and registration result images for forward and backward direction and the IC error were calculated. It was also computed the minimum Jacobian of each transformation.

Table 4.1 shows IC weight variation and IC error, NMI and minimum Jacobian associated with it for Patient X.

Table 4.1: IC error (mean, standard deviation and maximum), NMI and minimum Jacobian for different weight values of IC penalty term. Values related to patient X.

Penalty term	IC error (in mm)			NMI		min Jacobian	
IC	mean	std	max	Forward	Backward	Forward	Backward
0	1.2926	1.2871	11.6313	1.15823	1.15180	-0.04	0.43
0.002	0.7450	0.7232	6.9653	1.15510	1.15677	0.17	0.52
0.008	0.4419	0.4499	5.0675	1.15473	1.15783	0.18	0.47
0.01	0.3936	0.3997	4.8168	1.15484	1.15966	0.15	0.46
0.05	0.1597	0.1700	2.2248	1.15339	1.15591	0.27	0.43
0.1	0.0981	0.1103	1.9243	1.15112	1.16231	0.37	0.45
0.5	0.0212	0.0265	0.5091	1.14220	1.15502	0.52	0.56

Figure 4.1 shows examples of an overlap between the CBCT scan (yellow) and registration results (grey) when registrations were performed using

different values of IC weight.

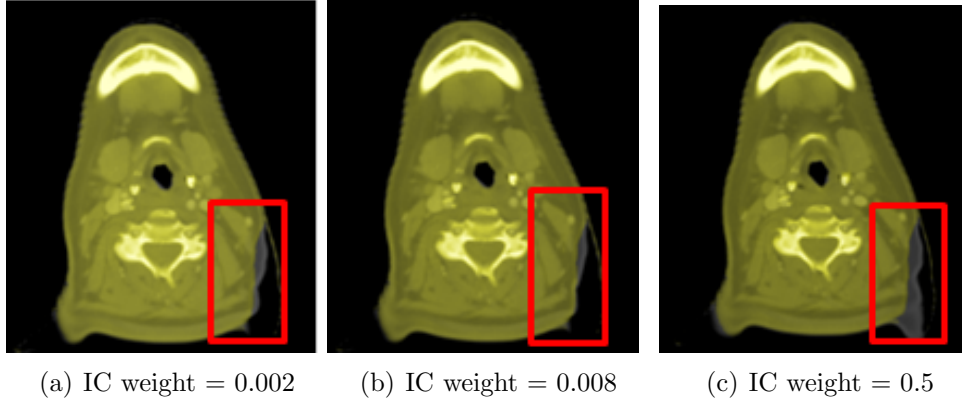


Figure 4.1: Transverse plane images of Patient X showing an overlap between CBCT (yellow) and deformed pCT (grey). Registration was performed using different values of IC weight: (a) 0.002, (b) 0.008 and (c) 0.5. Soft tissues are better aligned using smaller weights of IC penalty term (red square).

Symmetric registration algorithm showed to be very robust since a small variation of parameters did not cause big changes in the registration results. Increasing the weight of IC penalty term, reduces the IC error by forcing the transformations to be inversely consistent. On the other hand, in spite of much constrain weight, the transformation is not free to do deformations and the NMI decreases. IC penalty term values within $[0.0008, 0.01]$ seemed to represent a good compromise. Note that when not any constrain was used (IC penalty term = 0) the minimum Jacobian had a negative value which means that folding occurred. Similar results were found for Patient Y and Z.

Symmetric registrations were performed with a IC penalty term weight of 0.008 and a maximum number of 1000 iterations. In order to ensure a transformation 100% folding free we set a weight of a jacobian penalty term to 1% of the IC penalty term weight. Table 4.2 shows the final results for these parameters.

These results are very useful practically to understand the proper weight of symmetric registration parameters that is needed to achieve the best possible results for the registration of HN images. The optimal parameters found for the symmetric deformable registration were used in this study as

Table 4.2: IC error (mean, standard deviation and maximum), NMI and minimum Jacobian for the optimal registration parameters achieved.

Patient	IC error (in mm)			NMI		min Jacobian	
	mean	std	max	Forward	Backward	Forward	Backward
X	0.4409	0.4485	5.1418	1.15785	1.16833	0.14	0,38
Y	0.4992	0.5961	8.7574	1.17416	1.15986	0.14	0,35
Z	0.7101	0.8205	13.5251	1.16158	1.14069	0.001	0,21

inputs for all the following symmetric registrations performed.

4.2 EVALUATION OF DIFFERENT INVERSE TRANSFORM METHODS

This section presents the results of the assessment and evaluation of different inverse transform methods. The evaluation was based on the computation of similarity measures to ensure image matching quality and dose comparison to study the dosimetric effects. The 4 patients who had replan were included in this study (Patients X, Y, Z and K). Planning CT scan and CBCT image taken before replan were available.

4.2.1 SIMILARITY COMPARISON

First, we studied the performance of forward transformation T and backward/inverse transformation T^{-1} and then, their inverse-consistency when considered together.

In order to study registration performance in the forward direction, deformed pCT was compared with the CBCT image. Symmetric transform showed more similarity between deformed pCT and CBCT images than asymmetric transform (table 4.3). Both transformations were 100% folding free.

Overall asymmetric forward registration showed a better alignment of soft tissues and symmetric forward registration a better alignment of bone structures (figure 4.2).

Table 4.3: Registration performance in the forward direction.

Patient	Transform	NMI	Folding (%)
X	Asymmetric	1.16698	0
	Symmetric	1.17385	0
Y	Asymmetric	1.15046	0
	Symmetric	1.15714	0
Z	Asymmetric	1.15639	0
	Symmetric	1.16191	0
K	Asymmetric	1.13208	0
	Symmetric	1.13848	0

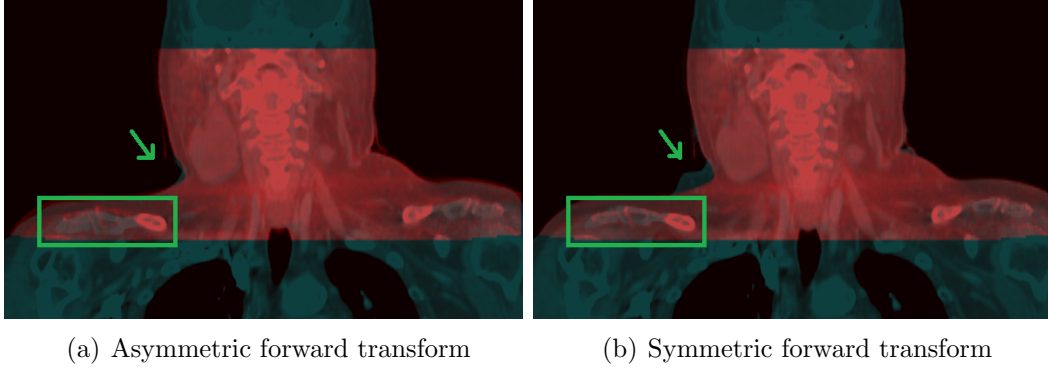


Figure 4.2: Coronal plane images of patient Z showing an overlap between CBCT (red) and deformed pCT (cyan). Registration was performed using an (a) asymmetric and (b) symmetric transform. Soft tissues are better aligned during asymmetric registration (green arrow) and bone structures are better aligned during symmetric registration (green square).

Deformed CBCT was compared with the pCT image to study registration performance in the backward direction. As in the forward direction, symmetric backward registration showed more similarity between images (table 4.4). All transformations were 100% folding free.

Estimate the inverse transform is the inverse of forward asymmetric transform therefore it showed a better alignment of soft tissues. Unlike it, backward symmetric transform, corresponding to the inverse of forward symmetric transform, showed a better alignment of bone structures (figure 4.3).

A simulated pCT was created in order to study the inverse consistency

Table 4.4: Registration performance in the backward direction.

Patient	Transform	NMI	Folding (%)
X	Asymmetric	1.15543	0
	Symmetric	1.16557	0
	Estimate 1	1.14809	0
	Estimate 2	1.15207	0
Y	Asymmetric	1.15349	0
	Symmetric	1.15689	0
	Estimate 1	1.14740	0
	Estimate 2	1.14718	0
Z	Asymmetric	1.11971	0
	Symmetric	1.13733	0
	Estimate 1	1.13012	0
	Estimate 2	1.13044	0
K	Asymmetric	1.12170	0
	Symmetric	1.12856	0
	Estimate 1	1.12156	0
	Estimate 2	1.12159	0

between forward T and backward/inverse T^{-1} transforms. Figure 4.4 shows the intensity difference images between the pCT and a simulated pCT generated by different inverse transforms. Since backward asymmetric transform is independently of the forward asymmetric approach, it gave the worst approximation of the pCT image. Estimate the inverse transforms gave the best approximation. Note that inside the CBCT field of view a better match occurred. Outside the CBCT field of view the transformations estimated the deformation per continuity with the one inside the field of view.

Two similarity measures were considered in order to analyse the similarity between pCT and simulated pCT. Estimate 1 transform gave the highest correlation value in all patients and backward asymmetric transform the lowest as can be seen in figure 4.5. The results are shown on a logarithm scale in order to proper see the differences between the different values. Normalized cross correlation values are presented in table 4.5.

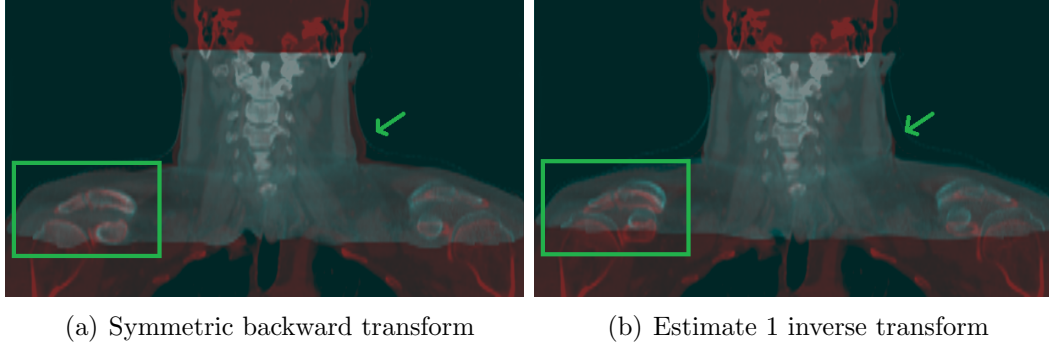


Figure 4.3: Coronal plane images of patient K showing an overlap between pCT (red) and deformed CBCT (cyan). Registration was performed using a (a) symmetric and (b) an estimate the inverse transform. Estimating the inverse transform shows a better alignment of soft tissues (green arrow) and backward symmetric shows a better alignment of bone structures.

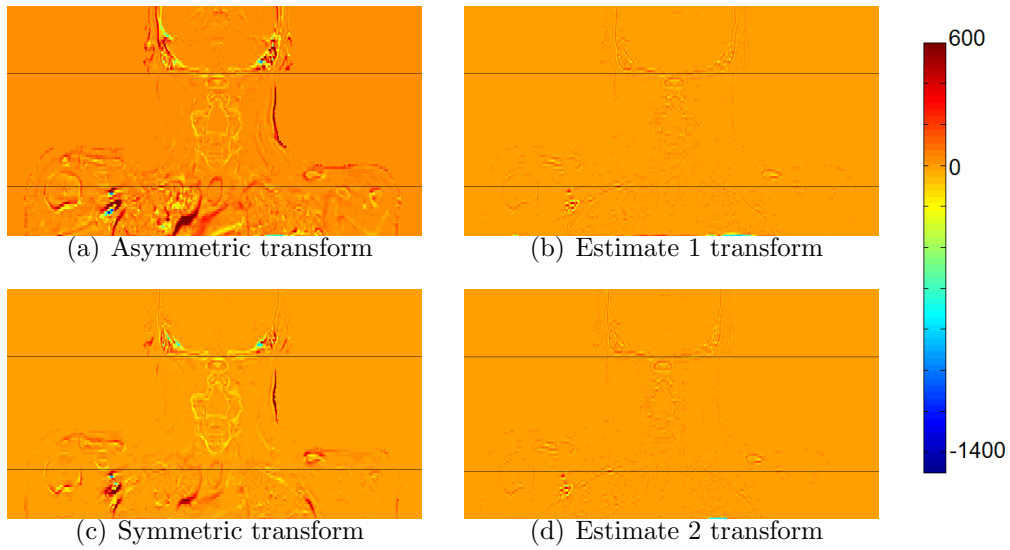


Figure 4.4: Coronal plane intensity difference images between pCT and simulated pCT generated by 4 different transforms: (a) backward asymmetric, (b) estimate 1, (c) backward symmetric and (d) estimate 2. Black horizontal lines represent the CBCT field of view and color scale is in CT intensity unit. Data sets from Patient Y.

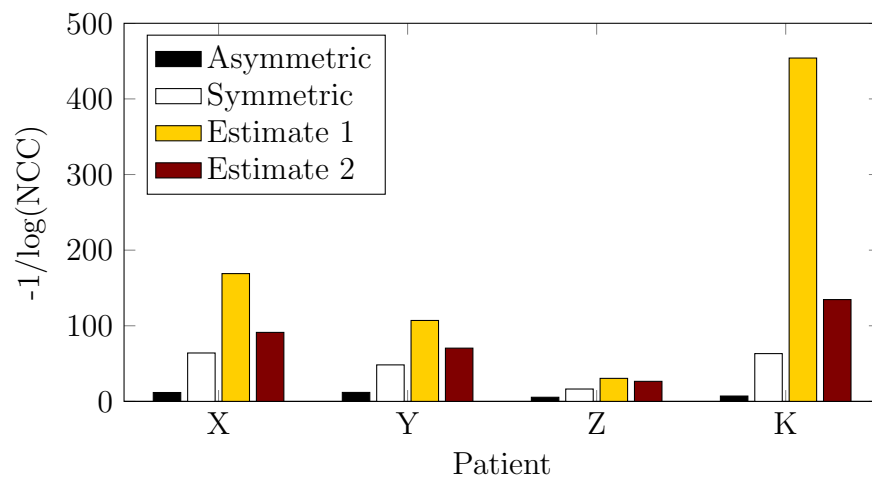


Figure 4.5: Normalized cross correlation between pCT and simulated pCT. The results are shown on a logarithm scale.

Table 4.5: Normalized cross correlation between pCT and simulated pCT generated by different transforms.

	Asymmetric	Symmetric	Estimate 1	Estimate 2
Patient X	0.9184	0.9845	0.9941	0.9891
Patient Y	0.9192	0.9795	0.9907	0.9859
Patient Z	0.8329	0.9407	0.9677	0.9630
Patient K	0.8682	0.9843	0.9978	0.9926

Similar results were observed for the sum of square intensity differences (figure 4.6). The best results were found by minimizing the SSD between images.

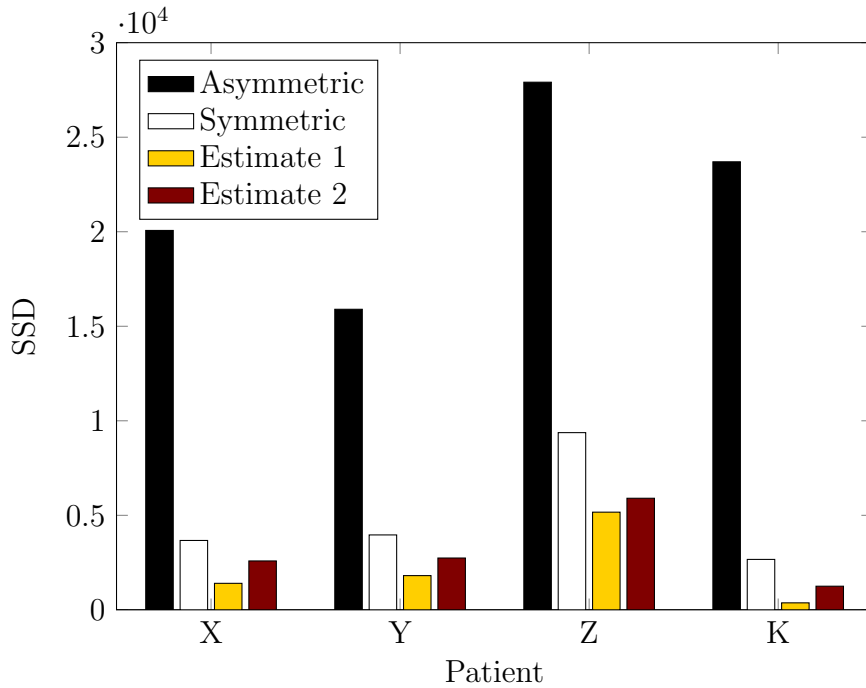


Figure 4.6: Sum of squared intensity differences between pCT and simulated pCT generated by different transforms.

The inverse consistent (IC) error between the composition of forward and inverse transformations is presented in table 4.6. If the deformation maps were true inverses, IC error would be zero.

The IC maximum error was much larger for the asymmetric algorithm (11.3848 mm) in comparison with the IC maximum error when using

Table 4.6: Inverse consistency error. Presented values are from different transforms and represent the median values over all subjects.

IC error (in mm)	Median values over all subjects		
	mean	standard deviation	maximum
Asymmetric	1.7546	1.7934	11.3848
Symmetric	0.4621	0.5125	5.8535
Estimate 1	0.0094	0.0034	0.0958
Estimate 2	0.0068	0.0069	0.1000

estimate the inverse methods (0.0958 mm).

In this analysis we studied the performance of the transformations when registration was performed in the (i) forward and (ii) backward direction and (iii) their consistency when considered together. In general, the results show that estimating the inverse is the most consistent method with a IC error of 0.009 mm (table 4.6), but it is not clear which is the most accurate. NMI results indicate symmetric to be more accurate, but visual results show that they can contain errors in the soft tissue which are not present in the asymmetric results (although these can contain errors in bony regions). But importantly all methods appear good in the high dose region so differences are unlikely to have much effect on calculated dose (as shown by study below, section 4.2.2). These results are important to study the effect that different inverse transforms have in the quality of the registration results and to ensure that transformations are true inverses.

4.2.2 DOSIMETRIC COMPARISON

Dosimetric effects were studied by mapping to the pCT space the recalculated dose in the deformed pCT using different inverse transforms. The comparison was performed between asymmetric/symmetric transforms and estimate 1 transform that consists in the method that we propose to be used in dose summation and was the method with the most consistent results (section 4.2). To find the most accurate method of calculating the real dose would require a real gold-standard, which would need to be a new kind of phantom which can use film or gel to measure the real dose, but can also move and deform realistically, and such a phantom does not yet exist (to our knowledge). A phantom with landmarks (or annotated scans) can be used to assess the spatial accuracy of the registrations, which is likely to lead to a more accurate dose calculation. The goal of

CHAPTER 4. RESULTS

validating the inverse transforms compared to physical reality is important however is beyond the scope of this study. Estimate 2 transform was not considered in this study since its results were similar to those given by estimate 1 transform (more efficiently implemented). Dose distributions comparison did not include the 5 mm on the edges of the patients since dose calculations are less accurate in that region and clinically not important.

Dose differences (DD) between inverse transform methods were found not significant (table 4.7) with a dose difference lower than 3% of the prescribed dose on 84.3% and 88.3% of the voxels for asymmetric and symmetric transforms, respectively, and they passed a 3% and 3 mm gamma pass criterion on 95.6% and 98.3%, respectively. Results are presented as median values over all subjects. With regard to the maximum absolute dose given to organs at risk (OAR) no significant differences were observed (table 4.8).

Table 4.7: Median values over all subjects for dose difference (DD) lower than 1%, 2% and 3% of the prescribed dose (pD) and gamma test with a pass criterion of 3% and 3mm. Results are shown for percentage of volume.

	Estimate 1 vs	Asymmetric	Symmetric
DD (%pD)	<1%	75.1%	78.7%
	<2%	84.3%	88.3%
	<3%	88.8%	92.5%
Gamma	3%/3 mm	95.6%	98.3%

Table 4.8: Maximum absolute dose differences in organs at risk (OAR). Results represent the median values over all subjects and they are in Gy unit.

	Estimate 1 vs	Asymmetric	Symmetric
Maximum DD in OAR	Brainstem	0.9 Gy	1.1 Gy
	Spinal Canal	0.3 Gy	0.2 Gy

Dose volume histograms (DVH) are useful to visualize the impact that dose distributions have on structures. Different dose distributions gave similar DVHs curves for each structure (figure 4.7).

No significant dosimetric differences were found between transforms. This results are important to conclude that different methods of computing

the inverse are consistent in terms of dosimetric effects.

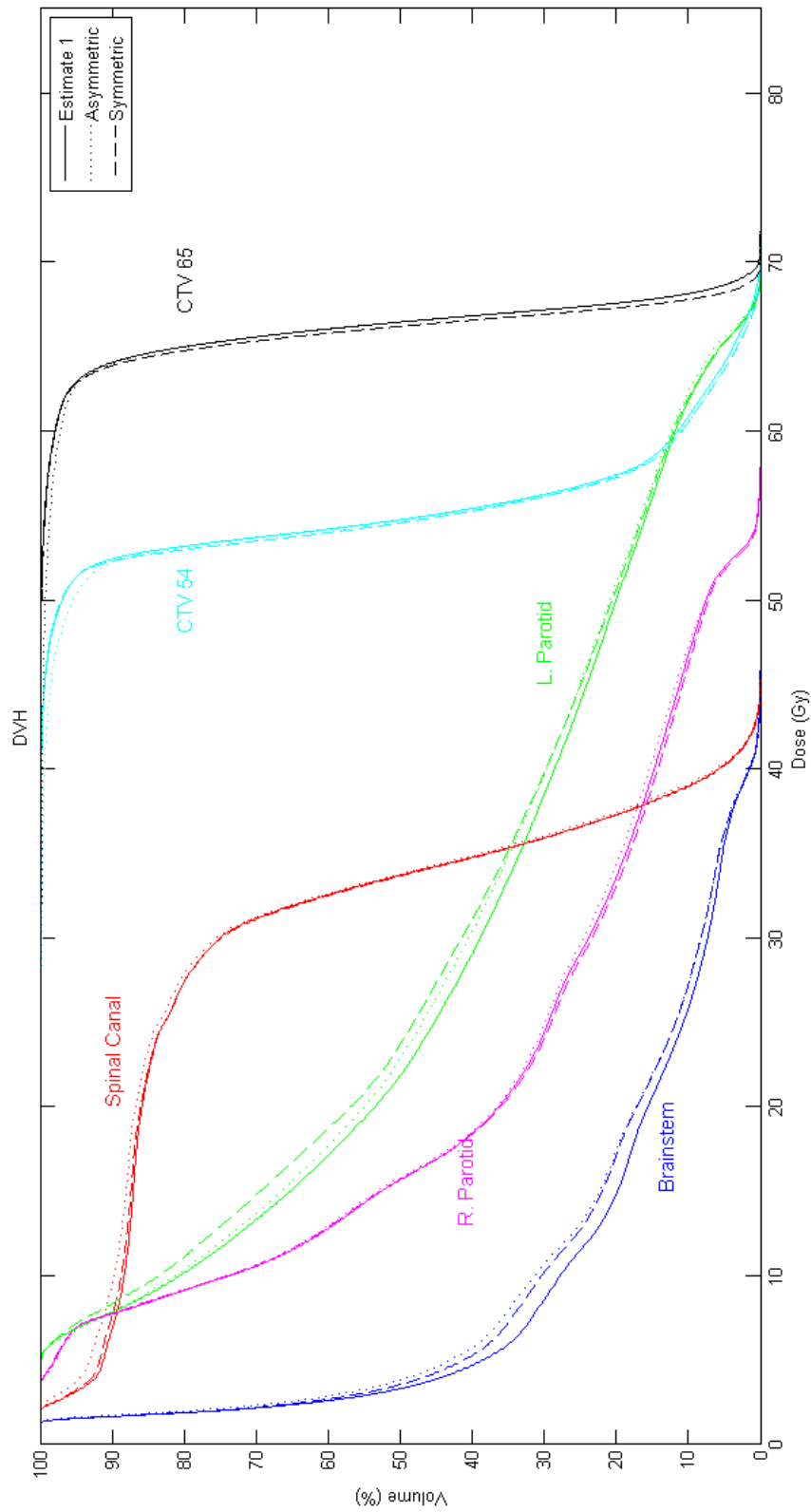


Figure 4.7: DVHs curves for different structures and dose distributions generated by asymmetric, symmetric and estimate inverse transforms, Patient Y.

4.3 CUMULATIVE DOSE CALCULATION

This chapter presents the results of the dose summation process proposed. Patient S who had no replan was considered in this study. Planning CT scan and 5 CBCTs images acquired during the treatment course were available.

Recalculated doses on weekly CBCTs were mapped to the pCT space using different inverse transforms allowing to compute the cumulative dose distributions while accounting for anatomic changes.

Cumulative dose distributions comparison was evaluated using the same tests and methodologies performed in section 4.2.2. The dose difference was lower than 3% of the prescribed dose on 97.0% and 96.4% of the voxels for estimate 1/asymmetric and estimate 1/symmetric transforms comparison, respectively, and they passed a 3% and 3 mm gamma test on 99.6% and 99.5% of the voxels, respectively (table 4.8).

Table 4.9: Dose difference (DD) lower than 1%, 2% and 3% of the prescribed dose (pD) and gamma test with a pass criterion of 3% and 3mm. Results are shown for percentage of volume.

	Estimate 1 vs	Asymmetric	Symmetric
DD (%pD)	<1%	88.2%	86.2%
	<2%	94.6%	93.6%
	<3%	97.0%	96.4%
Gamma	3%/3 mm	99.6%	99.5%

Maximum absolute dose differences in organs at risk (OAR) were found to be less than 1 Gy in both comparisons (table 4.10).

Table 4.10: Maximum absolute dose differences in organs at risk (OAR). Results are in Gy unit.

	Estimate 1 vs	Backward	Symmetric
Maximum DD in OAR	Brainstem	0.1 Gy	0.3 Gy
	Spinal Canal	0.8 Gy	0.8 Gy

In order to visualize dose differences over all patient's volume, dose difference images were generated. An example can be seen in figure 4.8. Main

differences were observed in the margins of the CBCT field of view (FoV) since deformations were estimated by continuity outside of it. In other words, by interpolating in the boundaries the deformation inside the FoV with the initial rigid alignment outside the FoV.

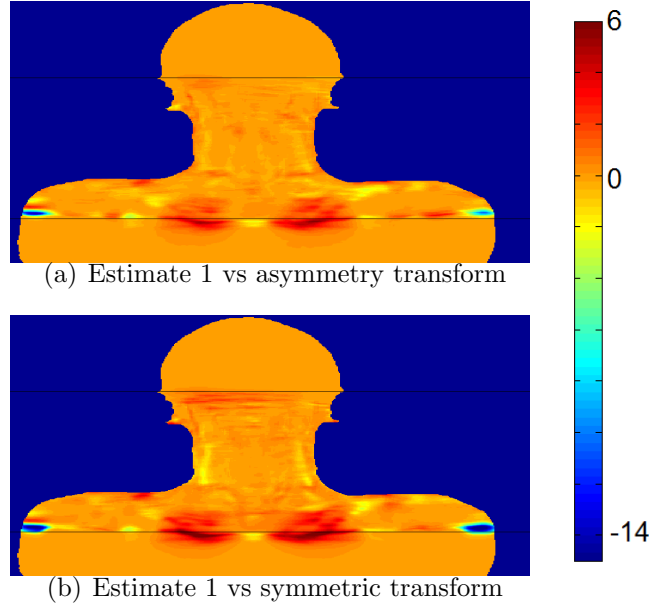


Figure 4.8: Coronal planes dose difference images between different transforms to compute the cumulative dose: (a) estimate 1 vs asymmetry, (b) estimate 1 vs symmetric. Black horizontal lines represent the CBCT field of view and color scale is in Gy unit.

The DVHs curves for the different dose distributions overlapped considerably and they are displayed in figure 4.8.

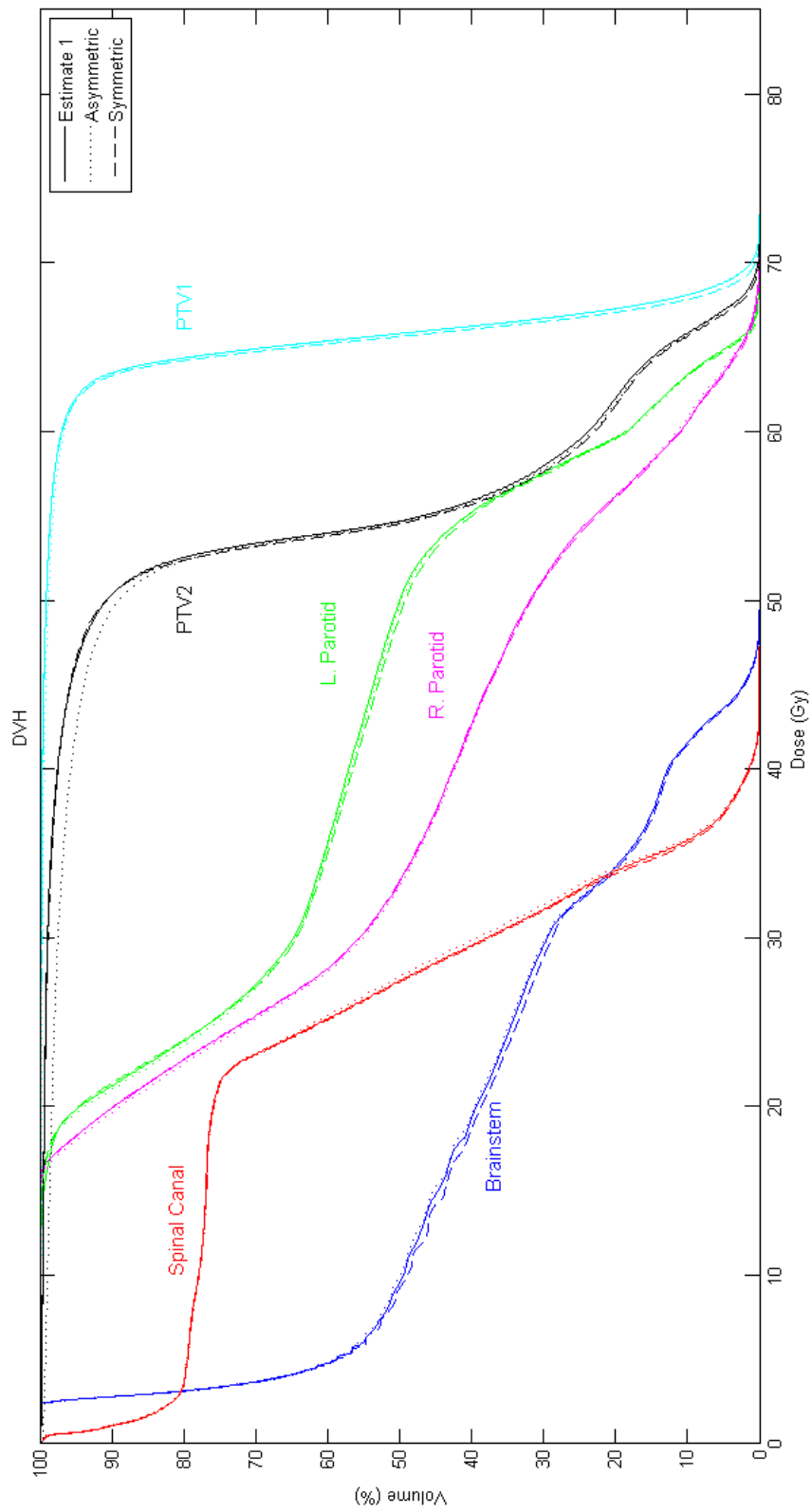


Figure 4.9: DVH for different structures and dose distributions generated by asymmetric, symmetric and estimate inverse transforms.

As in section 4.2.2, no significant differences were found between dose distributions. This results show that different methods of computing the inverse of a B-Spline transformation perform similar in terms of dose summation.

The time consumption for all the dose summation workflow will vary based on the number of CBCTs acquired, but in this case (with 5 CBCTs) it took approximately 30 minutes using method 1 of estimate the inverse approaches.

A Matlab code was written to implement the dose summation process (Appendix A.1). The user has to specify the inputs such as images and doses data sets, number total of fractions and the fraction at each CBCT was conducted. Guidelines for the dose summation tool use were provided in order to assist the clinicians (Appendix B).

4.4 COMPARISON OF DEFORMED pCT DOSE AND RECALCULATED DOSE

This section presents the results of recalculated dose in the deformed pCT, compared to deformed pCT dose. Deformed pCT dose was generated by applying the transformation that registers the pCT to the CBCT image to the pCT dose. The comparison was performed to evaluate if the recalculated dose performs similar to the dose that was planned to give (pCT dose accounting anatomic changes) and it can be use to assess the need to re-plan. Of the 4 patients who had replan, 3 (Patiet X, Y and Z) were included in this study. Planning CT scan and CBCT image taken before replan were available.

Dose difference and gamma analyses were computed to compare the two dose distributions (table 4.11). A dose difference lower than 3% of the prescribed dose on 88.8%, 88.5% and 77.0% of the voxels was found for patient X, Y, Z, respectively.

Regard to the maximum absolute dose differences in OAR the differences were minimal for patient X and Y, but a 6.8 Gy difference was found in spinal canal for patient Z (table 4.12). Indeed, such differences were also observed in the DVHs' curves. In figure 4.10 are displayed the respective

CHAPTER 4. RESULTS

Table 4.11: Dose difference (DD) lower than 1%, 2% and 3% of the prescribed dose (pD) and gamma test with a pass criterion of 3% and 3mm. Results are shown for percentage of volume.

		Patient X	Patient Y	Patient Z
DD (%pD)	<1%	72.4%	70.5%	61.2%
	<2%	83.2%	82.7%	70.7%
	<3%	88.8%	88.5%	77.0%
Gamma	3%/3 mm	97.5%	97.9%	88.5%

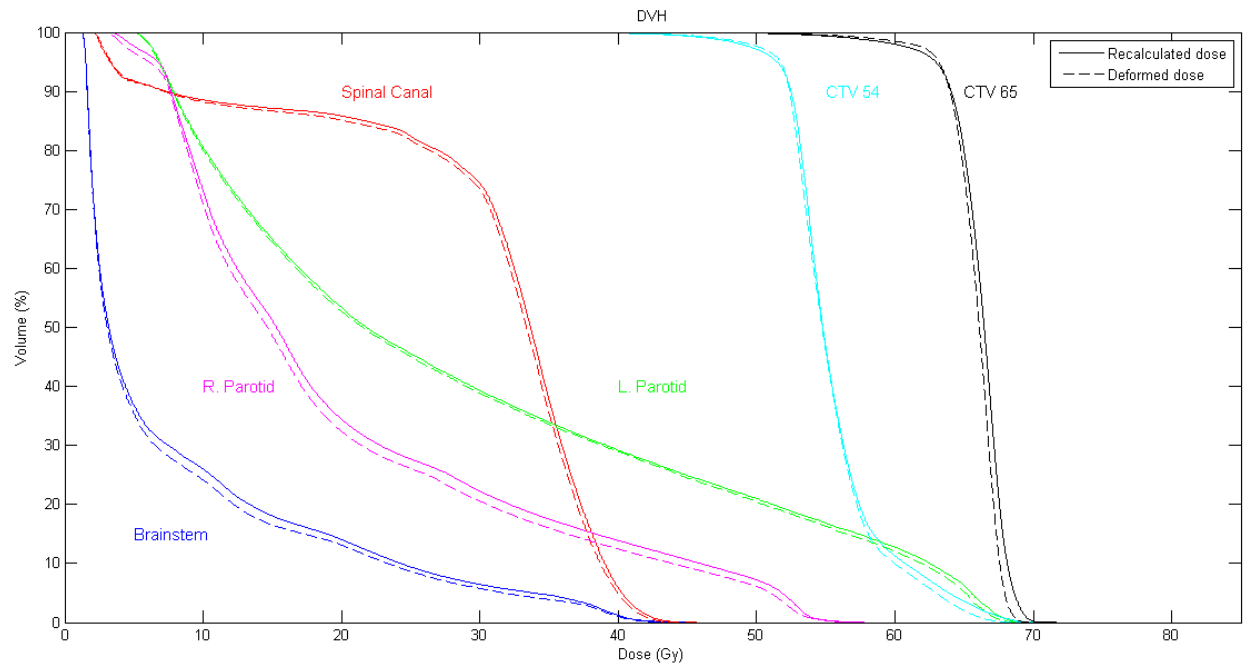
DVHs for patient X and Z.

Table 4.12: Maximum absolute dose differences in organs at risk (OAR). Results are shown in Gy unit.

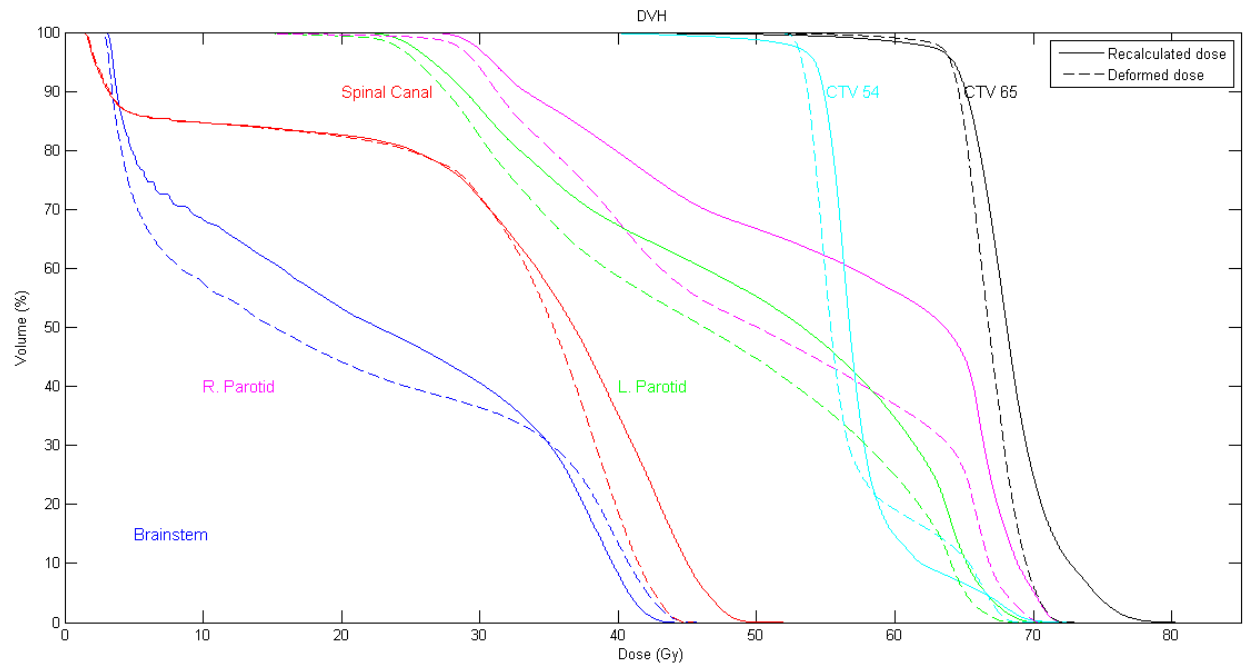
		Patient X	Patient Y	Patient Z
Maximum DD in OAR	Brainstem	0.1 Gy	1.5 Gy	1.8 Gy
	Spinal Canal	1.1 Gy	0.3 Gy	6.5 Gy

This substudy was done to compare the dose that was planned to give to the patients (deformed planning CT dose) with the recalculated doses. When significant discordance occur between the two dose distributions, the delivered dose might be considerably different from the initial plan dose and the patient should be considered for replan (for example, patient Z).

CHAPTER 4. RESULTS



(a) Patient X



(b) Patient Z

Figure 4.10: DVH for different structures and dose dose distributions for (a) patient X and (b) patient Z.

CHAPTER 5

DISCUSSION AND CONCLUSION

Different methods for estimating the cumulative dose received by radiotherapy patients while accounting for anatomic changes have been proposed. Yan *et al.* [53] using the finite element method developed a model for organ deformations during radiotherapy treatments in order to calculate the dose delivered within an organ of interest. Therefore, the external motion between different organs was not considered. Rosu *et al.* [54] estimated the cumulative dose distributions using trilinear interpolation by direct applying a deformation field to map the planning dose. However, the method showed to be inaccurate in steep dose gradient regions.

In order to overcome the interpolation errors, we recalculated the dose directly in the deformed geometry like Schaly *et al.* [55] and Heath *et al.* [62]. However, a correct point-to-point matching was not guaranteed in their studies since they used CT scans. Using CBCT scans creates additional problems because we need to first deform the pCT to perform the dose calculation, and then warp the dose back to the plan scan (they only had to warp the dose to the plan scan). Thus, inverse-consistency analysis are desired in order to ensure deformation maps that are true inverses when using CBCT scans.

The goal of this study was to assess and evaluate three different methods of computing the inverse of a B-Spline transformation (non-symmetric, symmetric and estimating the inverse methods) and present a method of calculating the daily and cumulative dose distributions by warping the recalculated doses in a deformed geometry back to the original pCT scan. Their performance was evaluated based on (i) visual inspection of registration results and computation of (ii) similarity measures to ensure

image matching quality, (iii) deformation field analysis and (iv) calculation of the inverse consistent error (IC) to ensure that transformations were physically plausible and true inverses.

Regarding inverse transformation performances, estimate the inverse of a B-Spline transformation method gave the most robust results in terms of inverse-consistency between the composition of forward and inverse transformations (figures 4.5, 4.6 and table 4.6), results comparable to the ones obtained by Varadhan *et al.* [63]. Backward asymmetric transformation gave the less consistent results since its computation is independently of forward transform. Although symmetric approach showed a higher image matching quality than estimate the inverse transform methods (table 4.4), differences were found to be not significant. In terms of inverse-consistency between the composition of forward and inverse transformations, estimate the inverse methods showed a mean IC error of 0.009 mm, and non-symmetric and symmetric approaches a error of 1.793 mm and 0.500, respectively. With regard to the dosimetric effects, results were found to be consistent between different inverse transforms. DVHs overlapped considerably (figure 4.7) and maximum absolute dose differences in organs at risk were found to be less than 1.1 Gy (table 4.8). The presented values represent the median values over all subjects.

We have developed a proof-of-principle method that computes the cumulative dose while accounting for variable anatomy and we showed that inverse strategies can be considered for dose mapping. We propose that estimating the inverse of a B-Spline transformation method has potential to be used in dose summation due to its fast implementation and robust results. All the dose summation process runs approximately in 30 minutes and so it can only be used in its current form for offline treatment planning revision.

Further developments on symmetric algorithms are needed in order to efficiently implement registration algorithms that are removed from bias. The accuracy of the registrations should also be validated for clinical purposes since at the moment previous work only validated the forward transformation. Additionally, a phantom study incorporating internal and external organs' deformation and with annotated landmarks is needed in order to assess the gold standard inverse transform method.

BIBLIOGRAPHY

- [1] E. K. Hansen, M. K. Bucci, J. M. Quivey, V. Weinberg, and P. Xia, “Repeat CT imaging and replanning during the course of IMRT for head-and-neck cancer,” *International journal of radiation oncology, biology, physics*, vol. 64, pp. 355–362, Feb. 2006. PMID: 16256277.
- [2] R. de Crevoisier, G. Louvel, G. Cazoulat, J. Leseur, C. Lafond, K. Lahbabi, C. Chira, and J.-L. Lagrange, “[image-guided radiotherapy: rational, modalities and results],” *Bulletin du cancer*, vol. 96, pp. 123–132, Jan. 2009. PMID: 19211367.
- [3] J. Hou, M. Guerrero, W. Chen, and W. D. D’Souza, “Deformable planning CT to cone-beam CT image registration in head-and-neck cancer,” *Medical physics*, vol. 38, pp. 2088–2094, Apr. 2011. PMID: 21626941.
- [4] U. Ueda, W. Hu, J. Pouliot, S. Yom, J. Quivey, M. Aubin, and J. Chen, “SU-DD-A3-02: the impact of cone-beam computed tomography (CBCT) artifacts on deformable image registration algorithms,” vol. 37, pp. 3091–3091, AAPM, 2010.
- [5] U. V. Elstrøm, B. A. Wysocka, L. P. Muren, J. B. B. Petersen, and C. Grau, “Daily kV cone-beam CT and deformable image registration as a method for studying dosimetric consequences of anatomic changes in adaptive IMRT of head and neck cancer,” *Acta oncologica (Stockholm, Sweden)*, vol. 49, pp. 1101–1108, Oct. 2010. PMID: 20831502.
- [6] S. Webb, *The Physics of Conformal Radiotherapy: Advances in Technology (PBK)*. Taylor & Francis, Dec. 2010.
- [7] S. Webb, “The physical basis of IMRT and inverse planning,” *The British journal of radiology*, vol. 76, pp. 678–689, Oct. 2003. PMID: 14512327.

BIBLIOGRAPHY

- [8] B. S. Teh, S. Y. Woo, and E. B. Butler, “Intensity modulated radiation therapy (IMRT): a new promising technology in radiation oncology,” *The oncologist*, vol. 4, no. 6, pp. 433–442, 1999. PMID: 10631687.
- [9] E. D. Podgorsak and International Atomic Energy Agency, *Radiation oncology physics: a handbook for teachers and students*. Vienna: International Atomic Energy Agency, 2005.
- [10] C. Nutting, D. P. Dearnaley, and S. Webb, “Intensity modulated radiation therapy: a clinical review.,” *British Journal of Radiology*, vol. 73, pp. 459–469, May 2000. PMID: 10884741.
- [11] M. Goitein, *Radiation Oncology: A Physicist’s-eye View*. Springer Science+Business Media, LLC, Jan. 2008.
- [12] N. Hardcastle, W. A. Tome, K. Foo, A. Miller, M. Carolan, and P. Metcalfe, “Comparison of prostate IMRT and VMAT biologically optimised treatment plans,” *Medical dosimetry : official journal of the American Association of Medical Dosimetrists*, vol. 36, no. 3, pp. 292–298, 2011. PMID: 20801014 PMCID: PMC2995847.
- [13] “Volumetric-modulated arc therapy: its role in radiation therapy - MedicalPhysicsWeb,” 2009. VMAT is currently a hot topic in radiotherapy. But it’s still lacking a universal theory relating the resulting dose distribution and clinical outcome to input parameters, explains Steve Webb.
- [14] D. L. Schwartz, A. S. Garden, J. Thomas, Y. Chen, Y. Zhang, J. Lewin, M. S. Chambers, and L. Dong, “Adaptive radiotherapy for head-and-neck cancer: initial clinical outcomes from a prospective trial,” *International journal of radiation oncology, biology, physics*, vol. 83, pp. 986–993, July 2012. PMID: 22138459.
- [15] P. Castadot, J. A. Lee, X. Geets, and V. Grégoire, “Adaptive radiotherapy of head and neck cancer,” *Seminars in Radiation Oncology*, vol. 20, pp. 84–93, Apr. 2010.
- [16] J. Barker, Jerry L, A. S. Garden, K. K. Ang, J. C. O’Daniel, H. Wang, L. E. Court, W. H. Morrison, D. I. Rosenthal, K. S. C. Chao, S. L. Tucker, R. Mohan, and L. Dong, “Quantification of volumetric and geometric changes occurring during fractionated radiotherapy for head-and-neck cancer using an integrated CT/linear accelerator system,” *International journal of radiation oncology, biology, physics*, vol. 59, pp. 960–970, July 2004. PMID: 15234029.

BIBLIOGRAPHY

- [17] Q. J. Wu, T. Li, Q. Wu, and F.-F. Yin, “Adaptive radiation therapy: technical components and clinical applications,” *Cancer journal (Sudbury, Mass.)*, vol. 17, pp. 182–189, June 2011. PMID: 21610472.
- [18] J. C. O’Daniel, A. S. Garden, D. L. Schwartz, H. Wang, K. K. Ang, A. Ahamad, D. I. Rosenthal, W. H. Morrison, J. A. Asper, L. Zhang, S.-M. Tung, R. Mohan, and L. Dong, “Parotid gland dose in intensity-modulated radiotherapy for head and neck cancer: is what you plan what you get?,” *International journal of radiation oncology, biology, physics*, vol. 69, pp. 1290–1296, Nov. 2007. PMID: 17967319.
- [19] J. L. Robar, A. Day, J. Clancey, R. Kelly, M. Yewondwossen, H. Hollenhorst, M. Rajaraman, and D. Wilke, “Spatial and dosimetric variability of organs at risk in head-and-neck intensity-modulated radiotherapy,” *International journal of radiation oncology, biology, physics*, vol. 68, pp. 1121–1130, July 2007. PMID: 17398025.
- [20] C. Han, Y.-J. Chen, A. Liu, T. E. Schultheiss, and J. Y. C. Wong, “Actual dose variation of parotid glands and spinal cord for nasopharyngeal cancer patients during radiotherapy,” *International journal of radiation oncology, biology, physics*, vol. 70, pp. 1256–1262, Mar. 2008. PMID: 18234431.
- [21] P. Castadot, X. Geets, J. A. Lee, and V. Grégoire, “Adaptive functional image-guided IMRT in pharyngo-laryngeal squamous cell carcinoma: is the gain in dose distribution worth the effort?,” *Radiotherapy and oncology: journal of the European Society for Therapeutic Radiology and Oncology*, vol. 101, pp. 343–350, Dec. 2011. PMID: 21724283.
- [22] I. C. o. R. U. a. Measurements, *Prescribing, recording, and reporting photon beam therapy*. International Commission on Radiation Units and Measurements, 1999.
- [23] R. Eiland, *Adaptive radiation therapy for head and neck cancer*. Master thesis, Technical University of Denmark, 2012.
- [24] N. G. Burnet, S. J. Thomas, K. E. Burton, and S. J. Jefferies, “Defining the tumour and target volumes for radiotherapy,” *Cancer Imaging*, vol. 4, pp. 153–161, Oct. 2004. PMID: 18250025 PMCID: PMC1434601.
- [25] W. R. Hendee and E. R. Ritenour, *Medical Imaging Physics, Fourth Edition*. Mar. 2003.

BIBLIOGRAPHY

- [26] A. Richter, Q. Hu, D. Steglich, K. Baier, J. Wilbert, M. Guckenberger, and M. Flentje, “Investigation of the usability of conebeam CT data sets for dose calculation,” *Radiation oncology (London, England)*, vol. 3, p. 42, 2008. PMID: 19087250.
- [27] D. L. G. Hill, P. G. Batchelor, M. Holden, and D. J. Hawkes, “Medical image registration,” *Physics in Medicine and Biology*, vol. 46, p. R1, Mar. 2001.
- [28] E. Schreibmann, P. Pantalone, A. Waller, and T. Fox, “A measure to evaluate deformable registration fields in clinical settings,” *Journal of applied clinical medical physics / American College of Medical Physics*, vol. 13, no. 5, p. 3829, 2012. PMID: 22955647.
- [29] J. A. Shackleford, N. Kandasamy, and G. C. Sharp, “On developing b-spline registration algorithms for multi-core processors,” *Physics in Medicine and Biology*, vol. 55, p. 6329, Nov. 2010.
- [30] W. R. Crum, T. Hartkens, and D. L. G. Hill, “Non-rigid image registration: theory and practice,” *The British journal of radiology*, vol. 77 Spec No 2, pp. S140–153, 2004. PMID: 15677356.
- [31] Q. Yang, *Analytic Regularization for B-spline Deformable Image Registration*. Master thesis in medical physics, Universität Heidelberg, Aug. 2011.
- [32] Z. Long, L. Yao, K. Chen, and D. Peng, “An improved exponential filter for fast nonlinear registration of brain magnetic resonance images,” *Progress in Natural Science*, vol. 19, pp. 759–767, June 2009.
- [33] T. Rohlfing, J. Maurer, C.R., D. Bluemke, and M. Jacobs, “Volume-preserving nonrigid registration of MR breast images using free-form deformation with an incompressibility constraint,” *IEEE Transactions on Medical Imaging*, vol. 22, no. 6, pp. 730–741, 2003.
- [34] J. R. McClelland, *Registration Based Respiratory Motion Models for use in Lung Radiotherapy*. PhD thesis, University College London, Mar. 2008.
- [35] P. J. Keall, S. Joshi, S. S. Vedam, J. V. Siebers, V. R. Kini, and R. Mohan, “Four-dimensional radiotherapy planning for DMLC-based respiratory motion tracking,” *Medical physics*, vol. 32, pp. 942–951, Apr. 2005. PMID: 15895577.

BIBLIOGRAPHY

- [36] D. Yang, H. Li, D. Low, J. Deasy, and I. El-Naqa, “A fast inverse consistent deformable image registration method based on symmetric optical flow computation,” in *2008 42nd Asilomar Conference on Signals, Systems and Computers*, pp. 1931–1935, 2008.
- [37] B. Papiez and B. Matuszewski, “Symmetric image registration with directly calculated inverse deformation field,” *Annals of the BMVA*, vol. 2012, no. 6, pp. 1–14, 2012.
- [38] M. Modat, M. J. Cardoso, P. Daga, D. Cash, N. C. Fox, and S. Ourselin, “Inverse-consistent symmetric free form deformation,” in *Biomedical Image Registration* (B. M. Dawant, G. E. Christensen, J. M. Fitzpatrick, and D. Rueckert, eds.), no. 7359 in *Lecture Notes in Computer Science*, pp. 79–88, Springer Berlin Heidelberg, Jan. 2012.
- [39] T. M. Deserno, *Biomedical Image Processing*. Springer, Jan. 2011.
- [40] J. Cooper, “Optical flow for validating medical image registration,” 2003.
- [41] J. A. Schnabel, C. Tanner, A. D. Castellano-Smith, A. Degenhard, M. O. Leach, D. R. Hose, D. L. G. Hill, and D. J. Hawkes, “Validation of nonrigid image registration using finite-element methods: application to breast MR images,” *IEEE transactions on medical imaging*, vol. 22, pp. 238–247, Feb. 2003. PMID: 12716000.
- [42] P. Jannin, J. M. Fitzpatrick, D. J. Hawkes, X. Pennec, R. Shahidi, and M. W. Vannier, “Validation of medical image processing in image-guided therapy,” *IEEE transactions on medical imaging*, vol. 21, pp. 1445–1449, Dec. 2002. PMID: 12588028.
- [43] G. P. Penney, J. Weese, J. A. Little, P. Desmedt, D. L. Hill, and D. J. Hawkes, “A comparison of similarity measures for use in 2-d-3-d medical image registration,” *IEEE transactions on medical imaging*, vol. 17, pp. 586–595, Aug. 1998. PMID: 9845314.
- [44] C. Studholme, D. Hill, and D. Hawkes, “An overlap invariant entropy measure of 3D medical image alignment,” *Pattern Recognition*, vol. 32, pp. 71–86, Jan. 1999.
- [45] N. D. Cahill, “Normalized measures of mutual information with general definitions of entropy for multimodal image registration,” in *Biomedical Image Registration* (B. Fischer, B. M. Dawant, and C. Lorenz, eds.),

BIBLIOGRAPHY

- no. 6204 in Lecture Notes in Computer Science, pp. 258–268, Springer Berlin Heidelberg, Jan. 2010.
- [46] N. Cahill, J. Schnabel, J. Noble, and D. Hawkes, “Revisiting overlap invariance in medical image alignment,” in *IEEE Computer Society Conference on Computer Vision and Pattern Recognition Workshops, 2008. CVPRW '08*, pp. 1–8, 2008.
- [47] J. C. Gee, J. B. A. Maintz, and M. W. Vannier, *Biomedical Image Registration: Second International Workshop, WBIR 2003, Philadelphia, PA, USA, June 23-24, 2003, Revised Papers*. Springer, Dec. 2003.
- [48] A. Myronenko, *Non-rigid image registration regularization, algorithms and applications*. Ph.D. thesis, Oregon Health & Science University, June 2010.
- [49] G. E. Christensen and H. J. Johnson, “Consistent image registration,” *IEEE transactions on medical imaging*, vol. 20, pp. 568–582, July 2001. PMID: 11465464.
- [50] S. B. Jiang, G. C. Sharp, T. Neicu, R. I. Berbeco, S. Flampouri, and T. Bortfeld, “On dose distribution comparison,” *Physics in medicine and biology*, vol. 51, pp. 759–776, Feb. 2006. PMID: 16467577.
- [51] J. Scherman, *Developement and evaluation of methods for comparison of dose distributions in radiotherapy using calculated, synthetic and simulated measured dose distributions*. Master’s degree, Lund University, 2009.
- [52] D. A. Low, W. B. Harms, S. Mutic, and J. A. Purdy, “A technique for the quantitative evaluation of dose distributions,” *Medical Physics*, vol. 25, no. 5, pp. 656–661, 1998.
- [53] D. Yan, D. Jaffray, and J. Wong, “A model to accumulate fractionated dose in a deforming organ,” *Int J Radiat Oncol Biol Phys*, vol. 44, pp. 665–675, June 1999.
- [54] M. Rosu, I. J. Chetty, J. M. Balter, M. L. Kessler, D. L. McShan, and R. K. Ten Haken, “Dose reconstruction in deforming lung anatomy: dose grid size effects and clinical implications,” *Medical physics*, vol. 32, pp. 2487–2495, Aug. 2005. PMID: 16193778.
- [55] B. Schaly, J. Kempe, G. Bauman, J. Battista, and J. Van Dyk, “Tracking the dose distribution in radiation therapy by accounting for variable anatomy,” *Phys Med Biol*, vol. 49, no. 5, pp. 791–805, 2004.

BIBLIOGRAPHY

- [56] M. Y. Y. Law and B. Liu, “DICOM-RT and its utilization in radiation therapy¹,” *Radiographics*, vol. 29, pp. 655–667, May 2009. PMID: 19270073.
- [57] S. Ourselin, A. Roche, G. Subsol, X. Pennec, and N. Ayache, “Reconstructing a 3D structure from serial histological sections,” *Image and Vision Computing*, vol. 19, pp. 25–31, Jan. 2001.
- [58] D. Rueckert, L. I. Sonoda, C. Hayes, D. L. Hill, M. O. Leach, and D. J. Hawkes, “Nonrigid registration using free-form deformations: application to breast MR images,” *IEEE transactions on medical imaging*, vol. 18, pp. 712–721, Aug. 1999. PMID: 10534053.
- [59] M. Modat, G. R. Ridgway, Z. A. Taylor, M. Lehmann, J. Barnes, D. J. Hawkes, N. C. Fox, and S. Ourselin, “Fast free-form deformation using graphics processing units,” *Computer methods and programs in biomedicine*, vol. 98, pp. 278–284, June 2010. PMID: 19818524.
- [60] C. Veiga, J. McClelland, K. Ricketts, D. D’Souza, and G. Royle, “Deformable registrations for head and neck cancer adaptive radiotherapy,” Image-Guidance and Multimodal Dose Planning in Radiation Therapy Workshop of the 15th International Conference on Medical Image Computing and Computer Assisted Intervention (MICCAI), 2012.
- [61] C. Veiga, J. McClelland, S. Moinuddin, K. Ricketts, M. Modat, S. Ourselin, and D. D’Souza, “Towards adaptive radiotherapy for head and neck patients: validation of an inhouse deformable registration algorithm,” IOP Conference Series, 2013.
- [62] E. Heath and J. Seuntjens, “A direct voxel tracking method for four-dimensional monte carlo dose calculations in deforming anatomy,” *Medical physics*, vol. 33, pp. 434–445, Feb. 2006. PMID: 16532951.
- [63] R. Varadhan, G. Karangelis, K. Krishnan, and S. Hui, “A framework for deformable image registration validation in radiotherapy clinical applications,” *Journal of applied clinical medical physics / American College of Medical Physics*, vol. 14, p. 4066, Jan. 2013. PMID: 23318394 PMID: PMC3732001.
- [64] S. Webb, “Motion effects in (intensity modulated) radiation therapy: a review,” *Physics in medicine and biology*, vol. 51, pp. R403–425, July 2006. PMID: 16790915.

BIBLIOGRAPHY

- [65] N. Lee, P. Xia, N. J. Fischbein, P. Akazawa, C. Akazawa, and J. M. Quivey, “Intensity-modulated radiation therapy for head-and-neck cancer: the UCSF experience focusing on target volume delineation,” *International journal of radiation oncology, biology, physics*, vol. 57, pp. 49–60, Sept. 2003. PMID: 12909215.
- [66] D. L. Schwartz and L. Dong, “Adaptive radiation therapy for head and neck cancer-can an old goal evolve into a new standard?,” *Journal of Oncology*, vol. 2011, Aug. 2010.
- [67] D. Yan, “Adaptive radiotherapy: merging principle into clinical practice,” *Seminars in radiation oncology*, vol. 20, pp. 79–83, Apr. 2010. PMID: 20219545.
- [68] V. Grégoire, R. Jeraj, J. A. Lee, and B. O’Sullivan, “Radiotherapy for head and neck tumours in 2012 and beyond: conformal, tailored, and adaptive?,” *The lancet oncology*, vol. 13, pp. e292–300, July 2012. PMID: 22748268.
- [69] T. Sanghangthum, S. Suriyapee, S. Srisatit, and T. Pawlicki, “Statistical process control analysis for patient-specific IMRT and VMAT QA,” *Journal of Radiation Research*, vol. 54, pp. 546–552, May 2013. PMID: 23220776 PMCID: PMC3650738.
- [70] G. E. Christensen, J. G. Kuhl, T. J. Grabowski, I. A. Pirwani, M. W. Vannier, J. S. Allen, and H. Damasio, “Introduction to the non-rigid image registration evaluation project (NIREP,” in *In Proceedings of SPIE*, p. 128–135, 2006.
- [71] S. Fomel, *Inverse B-spline interpolation*. 2000.
- [72] P. Rogelj and S. Kovačič, “Symmetric image registration,” *Medical Image Analysis*, vol. 10, pp. 484–493, June 2006.
- [73] D. B. Russakoff, T. Rohlfing, A. Ho, D. H. Kim, R. Shahidi, J. R. A. Jr, and C. R. M. Jr, “Evaluation of intensity-based 2D-3D spine image registration using clinical gold-standard data,” in *Biomedical Image Registration* (J. C. Gee, J. B. A. Maintz, and M. W. Vannier, eds.), no. 2717 in Lecture Notes in Computer Science, pp. 151–160, Springer Berlin Heidelberg, Jan. 2003.
- [74] T. Rohlfing, J. Maurer, C.R., D. Bluemke, and M. Jacobs, “Volume-preserving nonrigid registration of MR breast images using free-form

BIBLIOGRAPHY

- deformation with an incompressibility constraint,” *IEEE Transactions on Medical Imaging*, vol. 22, no. 6, pp. 730–741, 2003.
- [75] D. Skerl, D. Tomazevic, B. Likar, and F. Pernus, “Evaluation of similarity measures for reconstruction-based registration in image-guided radiotherapy and surgery,” *International journal of radiation oncology, biology, physics*, vol. 65, pp. 943–953, July 2006. PMID: 16751077.
- [76] H. Yan, R. Lei, J. Wu, F. Di, and F.-F. Yin, “Evaluation of image enhancement method on target registration using cone beam CT in radiation therapy,” *Clinical Medicine. Oncology*, vol. 2, pp. 289–299, Mar. 2008. PMID: 21892290 PMCID: PMC3161701.
- [77] J. Wu, M. Kim, J. Peters, H. Chung, and S. S. Samant, “Evaluation of similarity measures for use in the intensity-based rigid 2D-3D registration for patient positioning in radiotherapy,” *Medical physics*, vol. 36, pp. 5391–5403, Dec. 2009. PMID: 20095251.
- [78] T. Lehmann, A. Sovakar, W. Schmitt, and R. Repges, “A comparison of similarity measures for digital subtraction radiography,” *Computers in biology and medicine*, vol. 27, pp. 151–167, Mar. 1997. PMID: 9158921.
- [79] R. Kashani, M. Hub, J. M. Balter, M. L. Kessler, L. Dong, L. Zhang, L. Xing, Y. Xie, D. Hawkes, J. A. Schnabel, J. McClelland, S. Joshi, Q. Chen, and W. Lu, “Objective assessment of deformable image registration in radiotherapy: a multi-institution study,” *Medical physics*, vol. 35, pp. 5944–5953, Dec. 2008. PMID: 19175149.
- [80] C. Lee, K. M. Langen, W. Lu, J. Haimerl, E. Schnarr, K. J. Ruchala, G. H. Olivera, S. L. Meeks, P. A. Kupelian, T. D. Shellenberger, and R. R. Mañon, “Evaluation of geometric changes of parotid glands during head and neck cancer radiotherapy using daily MVCT and automatic deformable registration,” *Radiotherapy and oncology: journal of the European Society for Therapeutic Radiology and Oncology*, vol. 89, pp. 81–88, Oct. 2008. PMID: 18707786.
- [81] H.-M. Chen and P. K. Varshney, “Mutual information-based CT-MR brain image registration using generalized partial volume joint histogram estimation,” *IEEE transactions on medical imaging*, vol. 22, pp. 1111–1119, Sept. 2003. PMID: 12956266.
- [82] S. Suri and P. Reinartz, “On the possibility of intensity based registration for metric resolution SAR and optical imagery,” in *2th AG-ILE International Conference on Geographic Information Science* (J.-H.

BIBLIOGRAPHY

Haunert, B. Kieler, and J. Milde, eds.), (Hannover, Germany), pp. 1–19, June 2009.

Appendix

APPENDIX A

MATLAB CODE

A.1 DOSE SUMMATION PROCESS

```
1 %
2 %   COMPUTE THE CUMULATIVE DOSE DISTRIBUTION RECEIVED
   BY RADIOTHERAPY
3 %   PATIENTS USING ADVANCED DEFORMABLE REGISTRATION
   TECHNIQUES
4 %
5 %
6 % INPUTS:
7 %   Number total of fractions
8 %   Number total of CBCT
9 %   PlanningCT: nii file
10 %   Dose CT: nii file
11 %   Dose CT: dcm file
12 %   CBCT: nii file , after rigid alignment
13 %   Dose CBCT: nii file
14 %   CPP: nii file
15 %   Number of fractions
16 % OUTPUTS:
17 %   inverseCBCTdose
18
19 %%%%%%%%%%%%%%%%%%%%%%%%%%%%%%%%%%%%%%%%%%%%%%%%%%%%%%%%%%%%%%%%%%%%%%%%%%
20 %%%%%%%%%%%%%%%%%%%%%%%%%%%%%%%%%%%%%%%%%%%%%%%%%%%%%%%%%%%%%%%%%%%%%%%%%%
21 clc
22 clear all
```

APPENDIX A. MATLAB CODE

```

23
24
25 %———— load CT, doses CT, CBCT, doses CBCT, CPP
    registration —————
26
27 % Number total of fractions and of CBCT
28 totalfractions = input('Insert number total of
    fractions: ');
29 N = input('Insert number total of CBCT: ');
30
31 % CT and dose CT
32 [filenameCT,pathnameCT] = uigetfile('*.nii','Load NIFTI
    CT file ');
33 [filenameCTdose,pathnameCTdose] = uigetfile('*.nii','
    Load NIFTI DOSE CT file ');
34 filename_CTdose = [pathnameCTdose filenameCTdose];
35 [filenameCTdoseDICOM,pathnameCTdoseDICOM] = uigetfile('
    *.dcm','Load DICOM DOSE CT file ');
36 filename_CTdoseDICOM = [pathnameCTdoseDICOM
    filenameCTdoseDICOM];
37
38 % CBCT, dose CBCT, CPP registration and number of
    fractions
39 for i = 1:1:N
40
41     [filenameCBCT,pathnameCBCT] = uigetfile('*.nii',
        sprintf('Load NIFTI CBCT %d file after scanner
        alignment ',i));
42     [filenameCBCTdose,pathnameCBCTdose] = uigetfile('*.
        nii',sprintf('Load NIFTI DOSE CBCT %d file ',i));
43     [filenameCPP,pathnameCPP] = uigetfile('*.nii',
        sprintf('Load NIFTY CPP REGISTRATION %d ',i));
44
45     eval(sprintf('filename_CBCT%d = filenameCBCT;',i));
46     eval(sprintf('filename_CBCTdose%d =
        filenameCBCTdose;',i));
47     eval(sprintf('filename_CPP%d = filenameCPP;',i));
48
49     fraction(i) = input(sprintf('Insert number of
        fractions for CBCT %d: ',i));
50

```

APPENDIX A. MATLAB CODE

```
51 end
52
53
54 %----- run inverse
55 % Composition analysis
56 %obtain cpp
57 ref = filenameCTdose;
58 flo = filenameCT;
59 tmpcpp = 'tmpcpp.nii';
60 [status, result] = system(sprintf('reg_f3d -ref %s -flo
    %s -cpp %s -maxit 0 -ln 1', ref, flo, tmpcpp))
61
62 %conversion from control point grid to deformation
    field
63 tmpdef = 'tmpdef.nii';
64 [status, result] = system(sprintf('reg_transform -ref %
    s -cpp2def %s %s', ref, tmpcpp, tmpdef))
65
66 totalDose = 0;
67
68 for i = 1:1:N
69
70
71     % Inverse deformation field
72     tmpflo = filenameCT;
73     eval(sprintf('transRef = filename_CBCT%d;', i));
74     eval(sprintf('cpp = filename_CPP%d;', i));
75     defcpp = sprintf('defCPP-%d.nii', i);
76
77     [status, result] = system(sprintf('reg_transform -
        ref %s -cpp2def %s %s', transRef, cpp, defcpp))
78
79     defInverse = sprintf('defINVERSE%d.nii', i);
80     [status, result] = system(sprintf('reg_transform -
        ref %s -invDef %s %s %s', transRef, defcpp, tmpflo,
        defInverse))
81
82
83     % Applies inverse deformation field to doses
84     defcomp = sprintf('defcomp-%d.nii', i);
85     [status, result] = system(sprintf('reg_transform -
```

APPENDIX A. MATLAB CODE

```

    ref %s -comp3 %s %s %s',ref,defInverse,tmpdef,
    defcomp))

86
87     eval(sprintf('tmpflo2 = filename_CBCTdose%d;',i));
88     res = sprintf('inverseCBCTdose_%d.nii',i);
89     [status, result] = system(sprintf('reg_resample -
        ref %s -flo %s -def %s -res %s',ref,tmpflo2,
        defcomp,res))

90
91
92     %----- fraction dose
93     %read inverse dose using load_untouch_nii
94     eval(sprintf('nii_CBCTdose%d = load_untouch_nii(''
        inverseCBCTdose_%d.nii '');',i,i));
95     eval(sprintf('nii_CBCT_FRACTIONdose%d = (
        nii_CBCTdose%d.img).*(fraction(i)/totalfractions
        );',i,i));

96
97
98     %----- dose summation
99
100    eval(sprintf('totalDose = totalDose +
        nii_CBCT_FRACTIONdose%d;',i));

101
102
103 end
104
105
106 %----- create dose nifti file
107
108 header = load_untouch_nii(filename_CTdose);
109 header.img = totalDose;
110 save_untouch_nii(header,'DoseSummation.nii');
111
112
113 %----- create dose dicom file
114
115 % read CT dose using dicomread
116 dcm = dicomread(filename_CTdoseDICOM);
117 metadata = dicominfo(filename_CTdoseDICOM);
118

```

APPENDIX A. MATLAB CODE

```
119 % swap columns
120 new_nii = permute(header.img,[2 1 3]);
121
122 % size and class dcm
123 dcm_size = size(dcm);
124 new_dcm = zeros(dcm_size);
125 new_dcm(:,:,:) = new_nii;
126 new_dcm = uint32(new_dcm);
127
128 dicomwrite(new_dcm, 'DoseSummation.dcm', metadata, '
    CreateMode', 'copy');
```

APPENDIX B

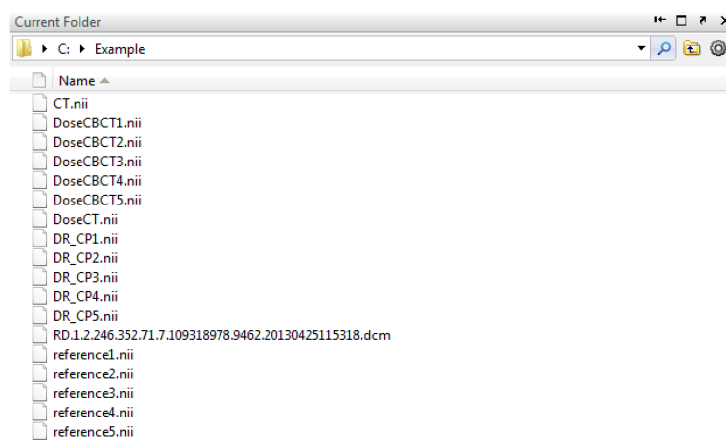
GUIDELINES FOR DOSE SUMMATION TOOL USE

APPENDIX B. GUIDELINES FOR DOSE SUMMATION TOOL USE

II – DEFORMABLE REGISTRATION FOR CLINICAL USE

Guidelines for DOSE SUMMATION

1. Computer: Run registration using Veiga et al. tool.
2. Eclipse: Export the DEFORMED CT dose in DICOM format.
Import DEFORMED CT and copy CT dose to DEFORMED CT. Calculate dose in DEFORMED CT.
3. NiftyView: Open the DEFORMED CT dose and CT dose and save them as .nii.
4. Ensure you have a directory with all the files necessary. Create a folder that contains the following:



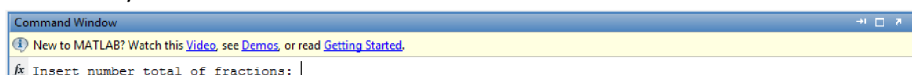
- “CT.nii” – the CT file in NIfTI format
 - “DoseCBCT#.nii” – the CBCT dose file in NIfTI format (see step 2,3)
 - “DoseCT.nii” – the CT dose file in NIfTI format (see step 3)
 - “DR_CP#.nii” – control point grid (CPP), output of registration (from Veiga et al. tool)
 - “RD.1.2.246.352.71.7.109318978.9462.20130425115318.dcm” – the CT dose file in DICOM format
 - “reference#.nii” – the CBCT file in NIfTI format after scanner alignment (from Veiga et al. tool)
5. MATLAB: Dose summation
 - On the “Command window” type:

Inverse

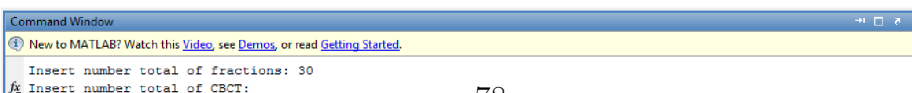
Example:



- A text will pop asking to insert the number total of fractions. Insert it and press Enter key.

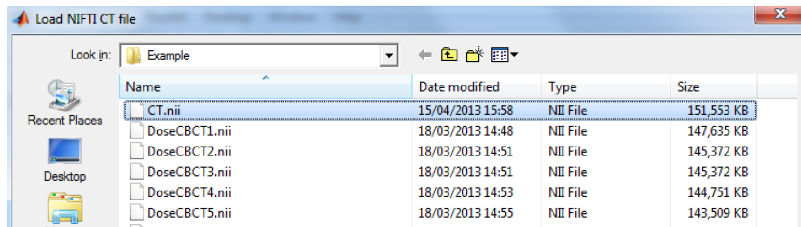


- It will also ask to insert the number total of CBCTs. Insert it and press Enter key.

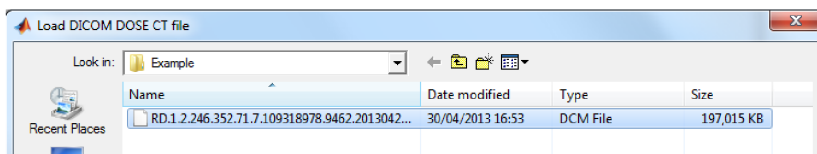
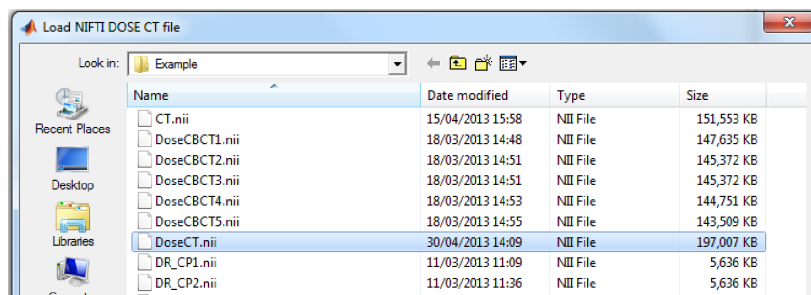


APPENDIX B. GUIDELINES FOR DOSE SUMMATION TOOL USE

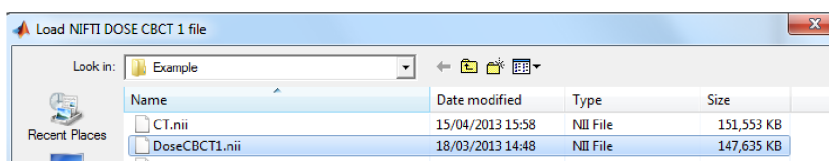
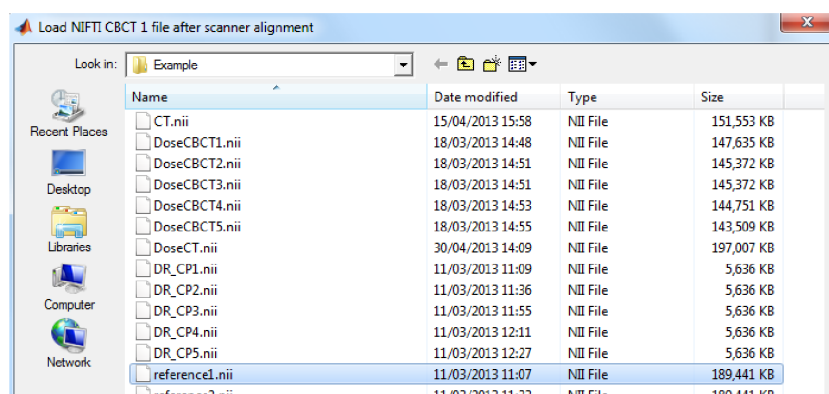
- A window will pop to load the NIFTI CT file. Select it with a double click.



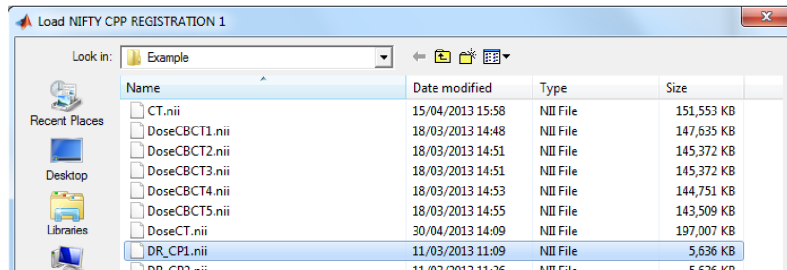
- Then select the following files: NIFTI dose CT and DICOM dose CT.



- For each CBCT you need to repeat the following procedures. Select the following files: NIFTI CBCT # after scanner alignment, NIFTI dose CBCT # and NIFTI CPP from registration #.



APPENDIX B. GUIDELINES FOR DOSE SUMMATION TOOL USE



- A text will pop asking to insert the number of fractions for the CBCT #. Insert it and press Enter key.



- The process will take around 3 minutes for each CBCT and it is finished when on the bottom left corner of the window the “Busy” message disappear.



- A lot of files were created. The ones that you are interested are:
 - “DoseSummation.dcm” – it can be imported back in Eclipse and it contains the sum of the doses of the CBCTs. Make sure that you delete the CT dose before you import it.
 - “DoseSummation.nii” – it can be opened in NiftyView and it contains the sum of the doses of the CBCTs.

